Neuron

Article

Transient and Persistent Representations of Odor Value in Prefrontal Cortex

Highlights

- Piriform cortex encodes odor identity, and only minor changes are observed after learning
- A transient neural representation of positive value emerges in the OFC during learning
- Persistent representations of positive and negative value emerge in the mPFC
- OFC and mPFC are required sequentially for the learning of appetitive associations

Authors

Peter Y. Wang, Cristian Boboila, Matthew Chin, ..., Nicole P. Stein, L.F. Abbott, Richard Axel

Correspondence

ra27@columbia.edu

In Brief

Wang et al. examine representations of odors in piriform cortex and two downstream areas, OFC and mPFC, during appetitive learning. They observe a representation of odor identity in piriform and representations of value in OFC and mPFC. Moreover, OFC and mPFC function sequentially in the learning of appetitive associations.

Wang et al., 2020, Neuron *108*, 209–224
October 14, 2020
https://doi.org/10.1016/j.neuron.2020.07.033

CellPress

Neuron

CellPress

Article

Transient and Persistent Representations of Odor Value in Prefrontal Cortex

Peter Y. Wang,[1,3] Cristian Boboila,[1,3] Matthew Chin,[1] Alexandra Higashi-Howard,[1,2] Philip Shamash,[1] Zheng Wu,[1] Nicole P. Stein,[1] L.F. Abbott,[1] and Richard Axel[1,2,4,*]

[1]The Mortimer B. Zuckerman Mind Brain Behavior Institute, Department of Neuroscience, Columbia University, New York, NY 10027, USA

[2]Howard Hughes Medical Institute, Columbia University, New York, NY 10027, USA

[3]These authors contributed equally

[4]Lead Contact

*Correspondence: ra27@columbia.edu

https://doi.org/10.1016/j.neuron.2020.07.033

SUMMARY

The representation of odor in olfactory cortex (piriform) is distributive and unstructured and can only be afforded behavioral significance upon learning. We performed 2-photon imaging to examine the representation of odors in piriform and in two downstream areas, the orbitofrontal cortex (OFC) and the medial prefrontal cortex (mPFC), as mice learned olfactory associations. In piriform, we observed that odor responses were largely unchanged during learning. In OFC, 30% of the neurons acquired robust responses to conditioned stimuli (CS+) after learning, and these responses were gated by internal state and task context. Moreover, direct projections from piriform to OFC can be entrained to elicit learned olfactory behavior. CS+ responses in OFC diminished with continued training, whereas persistent representations of both CS+ and CS− odors emerged in mPFC. Optogenetic silencing indicates that these two brain structures function sequentially to consolidate the learning of appetitive associations.

INTRODUCTION

Most organisms have evolved a mechanism to recognize olfactory information in the environment and process this information to create an internal representation of the external world. This representation must translate stimulus features into representations of value that guide appropriate behavior. Olfactory perception is initiated by the recognition of odorants by a large repertoire of receptors in the sensory epithelium (Buck and Axel, 1991; Godfrey et al., 2004; Zhang and Firestein, 2002). Individual sensory neurons in mice express only 1 of about 1,400 receptor genes, and neurons that express the same receptor project, with precision, to two spatially invariant glomeruli in the olfactory bulb (Mombaerts et al., 1996; Ressler et al., 1993, 1994; Vassar et al., 1994). Each odorant activates a unique combination of glomeruli, and the recognition of an odor requires integration of information from multiple glomeruli in higher olfactory centers.

The projection neurons of the olfactory bulb, the mitral and tufted cells, extend an apical dendrite into a single glomerulus and send axons to several telencephalic areas, including significant input to piriform cortex (Price and Powell, 1970). Anatomic tracing reveals that individual glomeruli discard the spatial patterning of the bulb and diffusely innervate the piriform (Ghosh et al., 2011; Sosulski et al., 2011). Electrophysiological and optical recordings demonstrate that individual odorants activate subpopulations of neurons distributed across the piriform without apparent spatial preference (Illig and Haberly, 2003; Iurilli and Datta, 2017; Poo and Isaacson, 2009; Rennaker et al., 2007; Stettler and Axel, 2009; Sugai et al., 2005; Zhan and Luo, 2010). Moreover, exogenous activation of an arbitrarily chosen ensemble of piriform neurons can elicit behaviors of contrasting valence that depend on learning (Choi et al., 2011). These observations are consistent with a model in which individual piriform cells receive convergent input from a random collection of glomeruli (Davison and Ehlers, 2011; Miyamichi et al., 2011; Stettler and Axel, 2009). In this model, odor representations in piriform can only be afforded behavioral significance upon learning.

The piriform cortex sends projections to numerous brain regions, including the amygdala, hippocampus, and prefrontal cortex, and is anatomically poised to accommodate the transformation of sensory representations into representations of value that can lead to appropriate behavioral output (Chen et al., 2014; Diodato et al., 2016; Johnson et al., 2000; Price, 1985; Schwabe et al., 2004). Neurons in orbitofrontal cortex (OFC) in both rodents and primates represent value but also encode other task variables, including stimulus identity, motor action, confidence, internal state, and task context (Feierstein et al., 2006; Gottfried et al., 2003; Hirokawa et al., 2019; Kepecs et al., 2008; Lipton et al., 1999; Namboodiri et al., 2019; Padoa-Schioppa and Assad, 2006; Ramus and Eichenbaum, 2000; Schoenbaum et al., 1998, 1999; Schoenbaum and Eichenbaum,

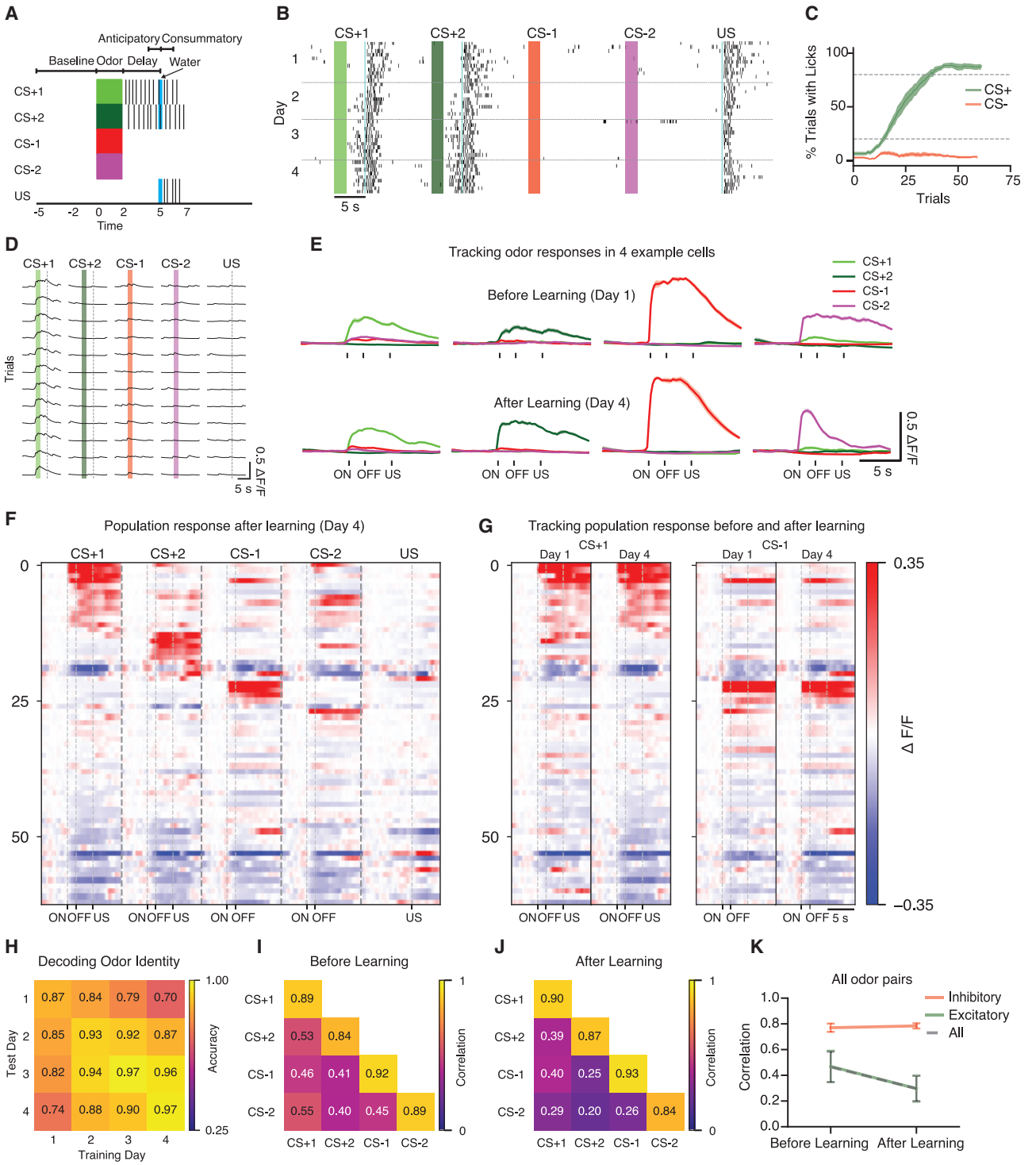

Figure 1. Odor Representations in Piriform Cortex Are Largely Unchanged during Learning

(A) Schematic of the single-phase discrimination learning paradigm used for imaging. Odor is presented for 2 s (colored bars), followed by a 3-s delay and US for CS+ odors (blue line). In US-only trials, odors are not presented before US. Black rasters denote single licks.

(B) Anticipatory licking behavior in response to CS+ odors, but not CS− odors, after learning in a single mouse. Horizontal lines separate the 4 training days.

(C) Summary of training data for the appetitive odor discrimination task (n = 14 mice, piriform and OFC single-phase imaging experiments). Percentage of trials with anticipatory licking in response to CS+ (green) and CS− (red) odors and learning criteria (dotted lines) for CS+ (top) and CS− (bottom). Here and below, shading indicates ± 1 SEM.

(legend continued on next page)

1995; Thorpe et al., 1983; Tremblay and Schultz, 1999). Lesion experiments implicate OFC in the updating of learned information, but these studies did not reveal a role for OFC in simple associative learning (Bissonette et al., 2008; Burke et al., 2008; Chudasama and Robbins, 2003; Gallagher et al., 1999; Izquierdo et al., 2004; Ostlund and Balleine, 2007; Schoenbaum et al., 2002; Stalnaker et al., 2007). Medial prefrontal cortex (mPFC) has been implicated in simple associative learning and the remodeling of learned information (Bari et al., 2019; Birrell and Brown, 2000; Bissonette et al., 2008; Chudasama and Robbins, 2003; Ferenczi et al., 2016; Kim et al., 2017; Kitamura et al., 2017; Ostlund and Balleine, 2005; Otis et al., 2017). However, in recent studies, a neural representation of rewarded auditory stimuli was identified in both OFC and mPFC, and silencing of these brain structures elicited deficits in the acquisition and expression of learned behavior (Namboodiri et al., 2019; Otis et al., 2017).

We have performed two-photon endoscopic imaging in piriform, OFC, and mPFC during appetitive associative conditioning to identify brain structures that exhibit changes in their neural representations upon olfactory learning (Barretto et al., 2009; Denk et al., 1990; Jung et al., 2004). Optogenetic silencing was then used to discern possible roles for these representations in associative conditioning. These experiments demonstrate a representation of odor identity in piriform, a transient representation of positive value in the OFC, and a persistent representation of positive and negative value in the mPFC.

RESULTS

Representation of Odor Identity in Piriform Cortex

We examined odor representations in piriform cortex while mice learned a classical appetitive odor discrimination task. Head-fixed mice were exposed to two conditioned stimuli (CS+), odors that predicted a water reward delivered after a short delay and to two unrewarded conditioned stimuli (CS−) (Figure 1A). In separate trials, the mice received a water reward (water delivery [US]) without prior odor delivery. After three to four training sessions, nearly all mice displayed anticipatory licking in response to the CS+ odors in more than 80% of the trials (13/14 mice) and licked in fewer than 20% of the CS− trials (14/14 mice) (Figures 1B and 1C). We imaged neural activity by 2-photon microscopy during training in mice expressing GCaMP6s in excitatory neurons in the piriform (Barretto et al., 2009; Chen et al., 2013; Denk et al., 1990; Jung et al., 2004). Mice bearing a Cre-dependent GCAMP6s gene (Rosa-Flex-GCaMP6s; Madisen et al., 2015) were crossed to mice expressing Cre under the control of the Vglut2 promoter (Vglut2-ires-Cre; Vong et al., 2011). In these mice, more than 80% of excitatory neurons in the piriform express GCaMP6s (Figures S1A–S1F). The activity of piriform neurons in six mice was stably recorded during 4 sessions of training spread over a week (Videos S2 and S3). Four of these mice were also imaged on exposure to a different set of odors in the absence of learning (passive odors).

Before learning, the four odors each activated a distinct and distributed ensemble of piriform neurons (Figures 1D–1F). As described previously (Stettler and Axel, 2009), each odor activated an average of 16% of the neurons (Figure S2A). The response properties of the neurons exhibited only small changes over 4 days of learning (Figure 1G). A linear decoder trained on population activity before learning was able to distinguish the identities of the four odors using population activity after learning (day 4 of training) with 74% accuracy (Figures 1H and S2B). Similar stability was also observed across 4 days of passive exposure to odor (Figure S2F).

However, we observed some changes in the response properties in piriform. Correlations between all pairs of odor ensembles were low before learning (Figures 1I and 1K; Pearson's correlation: 0.46) and decreased even further after learning (Figures 1J and 1K; Pearson's correlation: 0.30, $p < 0.001$, Wilcoxon signed-rank test). In accordance with these data, the classification of odor identity using a linear decoder improved from 87% accuracy on day 1 of training to 97% accuracy on day 4 of training (Figure 1H; $p < 0.05$, Wilcoxon signed-rank test). The increase in selectivity was observed for both CS+ and CS− odors and was also observed after 4 days of passive odor exposure (Figures S2F–S2K). This suggests that the increase in odor selectivity is a consequence of repeated experience, not of associative learning. However, we observed learning-related changes in the response to CS+ odors. An increase in response amplitude after learning was observed for CS+ odors (Figure S2C; 31%, $p < 0.05$), whereas changes to CS− and passive odors were not statistically significant (Figures S2D and S2E). We note that our imaging experiments were performed in the anterior piriform, and differences have been reported between electrophysiological responses of anterior piriform and those of posterior piriform during odor learning (Calu et al., 2007).

An inhibitory response is observed in 18% of neurons upon odor exposure (Figure S2L). However, the inhibitory response to odors is non-selective (Figures 1F, 1K, and S2G–S2K). CS+ and CS− odors elicit inhibition in a highly overlapping set of

(D) Individual odor trials collected from a single piriform neuron on day 4 of training.
(E) Trial-averaged responses to odors of 4 piriform neurons before learning (top row, day 1 of training) and after learning (bottom row, day 4 of training). ON, odor onset; OFF, odor offset.
(F) PSTH (peristimulus time histogram) of piriform responses after learning for one mouse. Each row denotes a single cell's trial-averaged responses to the four odors and water.
(G) PSTH of piriform responses before learning and after learning to CS+1 (left) and to CS−1 (right). Cells are tracked across days in the same row.
(H) Accuracy of decoding the identities of the four odors from population activity within and across training days (n = 6 mice). Decoding accuracy: train/test on day 1, 0.87; train/test on day 4, 0.97; Wilcoxon signed-rank test, $p < 0.05$; chance accuracy: 0.26. See STAR Methods.
(I and J) Correlation of activity evoked by all odor pairs before learning (I) and after learning (J). See STAR Methods.
(K) Correlation of odor-evoked population responses for all odor pairs before and after learning. Green, correlation of excitatory responses: 0.47 on day 1, 0.30 on day 4, $p < 0.001$; red, correlation of inhibitory responses: 0.77 on day 1, 0.78 on day 4, $p = 0.83$; gray, correlation of all responses: 0.46 on day 1, 0.30 on day 4, $p < 0.001$.
See also Figure S4.

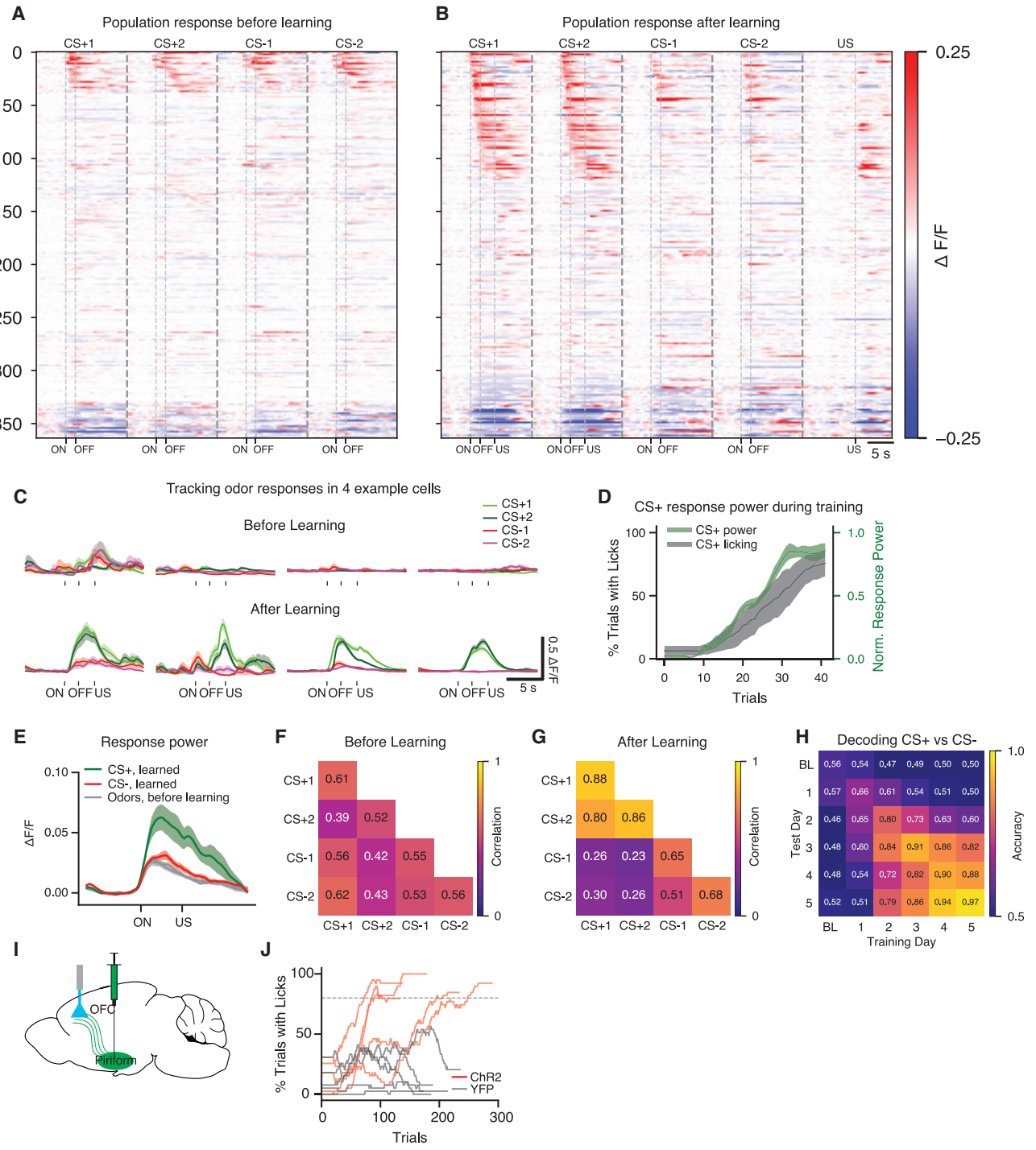

Figure 2. A CS+ Representation Emerges in the OFC after Learning

(A and B) PSTH of OFC responses for all animals (n = 5) before learning (A) and after learning (B). Responses before and after learning are sorted independently by response onset to CS+ odors.

(C) Trial-averaged responses of 4 example OFC cells to odors before learning (top) and after learning (bottom). ON, odor onset; OFF, odor offset. Here and below, shading indicates ± 1 SEM.

(D) Excitatory response power of OFC neurons to CS+ odors (green) versus percentage of CS+ trials with anticipatory licks (gray) during training.

(E) Average excitatory response power of OFC neurons to CS+ and CS− odors before learning (all odors, gray) and after learning (CS+, green; CS−, red). n = 5 mice. Here and below, see Table S1 for values.

(F and G) Within-day correlations between odor ensembles before learning (F) and after learning (G).

(legend continued on next page)

neurons before and after learning (Figure 1K; correlation: before, 0.77; after, 0.78, p = 0.83, Wilcoxon signed-rank test). This suggests that inhibitory responses are not specific, do not discriminate odor identity, and may be a consequence of specific excitation. Altogether, these results demonstrate that despite small increases in discriminability upon continued odor exposure, odor representations in piriform were largely unchanged during learning. Neural instantiations of learning must therefore occur downstream of piriform.

A Representation of Value in OFC

The piriform cortex sends axons to numerous brain regions, with extensive projections to OFC (Chen et al., 2014; Price, 1985). We therefore asked whether appetitive odor learning elicits changes in the representation of odors in OFC. We imaged the activity of 364 OFC neurons in 5 animals across 4–5 training days. Before learning, the four odors each activated an average of 11% of the neurons in OFC (Figures 2A and S3A). The responses were non-selective, inconsistent, and low in amplitude (Figures 2A and 2C).

We observed a striking change in the neuronal response to CS+ odors as learning proceeded (Figures 2B and 2C). After learning, 29% of the OFC neurons acquired consistent, high-amplitude excitatory responses to each of the two CS+ odors (Figure S3A; $p < 0.01$, Wilcoxon signed-rank test). The mean excitatory response amplitude (response power) evoked by CS+ odors increased with learning (Figure 2D) and plateaued at a value two-fold higher (210%) than the response observed before learning (Figure 2E; $p < 0.01$, Wilcoxon signed-rank test). After learning, 72% of neurons responsive to one CS+ odor also responded to the second CS+ odor (Figure S3B; overlap: before, 25%; after, 72%, $p < 0.05$, Wilcoxon signed-rank test). Moreover, the amplitude and duration of responses to the two CS+ odors in a given neuron were similar (Figures S3C and S3D). In accordance with these data, the population responses of the two CS+ odors were highly correlated after learning (Figures 2F, 2G, and S3E; correlation: before, 0.40; after, 0.80, $p < 0.01$, Wilcoxon signed-rank test). In contrast, CS− odors continued to elicit sparse, inconsistent, and low-amplitude responses (Figures 2B, 2C, 2E, and S3A). We also observe that inhibitory responses increase during learning, but these responses are non-selective (Figures S3E–S3G) and increase with excitation (Figures S3H and S3I). We have considered the possibility that the neural responses we observe in the OFC may reflect motor activity or licking, but multiple observations described in Supplemental Information render this alternative unlikely (Figure S4). Altogether, these results suggest that projections from the CS+ representation in piriform to the OFC are reinforced during learning.

We performed decoding analysis to further examine the effect of learning on the OFC representation. A linear decoder trained on population responses before learning decoded odor identity in the OFC at an accuracy slightly higher than chance (accuracy: 36%; shuffled accuracy: 26%, $p < 0.01$. Wilcoxon signed-rank test). A decoder trained on population responses after learning distinguished between rewarded and unrewarded odors with greater than 95% accuracy (Figures 2H and S3J; accuracy: before learning, 0.56; after learning, 0.97, $p < 0.05$). In contrast, a decoder classified the identity of the two CS+ odors (Figure S3K; CS+: before, 61%; after, 64%, p = 0.69) and the identity of the two CS− odors (Figure S3L; CS−: before, 61%; after, 59%, p = 0.89) at close to chance, and this did not change significantly with learning. This is in accordance with our observation that after learning, the population activities between the two CS+ odors are highly correlated (Figures 2G and S3E). These data suggest that the representation of odor identity in piriform is discarded in the OFC, and a representation of positive value emerges with learning.

Entrainment of Direct Piriform Projections to OFC

We next asked whether associative learning reinforces the projections from piriform to OFC. In previous experiments, we used virus to generate a random ensemble of neurons in piriform that express channelrhodopsin (ChR2). Activation of this ChR2 ensemble in piriform, when paired with reward, results in appetitive associative conditioning (Choi et al., 2011). We therefore determined whether entrainment of piriform projections to the OFC, rather than piriform cell bodies, can drive appetitive learning. ChR2 was expressed in a random subpopulation of neurons in anterior piriform. We then paired the optogenetic activation of ChR2-expressing piriform projections in the OFC with water reward (Figure 2I). In this training paradigm, entrainment resulted in anticipatory licking in all 5 ChR2 mice, whereas none of the 5 control mice expressing YFP were able to learn (Figure 2J). An average of 128 trials of laser entrainment was required to elicit learning (Figure 2J). This is almost twice the number of trials required to learn with a single CS+ odor (Figures 5B and 5C; 70 trials with odor), perhaps reflecting the small number of ChR2-expressing cells when compared with the size of a piriform odor ensemble. This experiment demonstrates that the activation and entrainment of direct inputs from piriform to OFC is capable of driving associative learning. This result suggests, but does not prove, a direct transformation of odor identity in the piriform to odor value in the OFC.

The OFC Representation Reflects Changes in Value

If the value of an odor changes, the representation of value in OFC should also change (Roesch et al., 2007; Schoenbaum et al., 1999; Thorpe et al., 1983). We therefore recorded neural responses in OFC during reversal learning. Mice were trained with 2 CS+ and 2 CS− odors in the appetitive learning task, and then the odor-reward contingencies were reversed. After reversal, the mice displayed anticipatory licking in response to the old CS−

(H) Accuracy of decoding predictive value (CS+ odors versus CS− odors) from OFC population activity within and across training days.
(I) Schematic of the piriform output optogenetic entrainment experiment. ChR2-expressing virus (green) is injected into the anterior piriform, and piriform terminals in the OFC are photostimulated (blue).
(J) Percentage of trials with anticipatory licking in response to photoillumination in animals expressing ChR2 (red, n = 5 mice) or YFP (yellow fluorescent protein) (black, n = 5 mice). The dotted line indicates the learning criterion.
See also Figures S3 and S4.

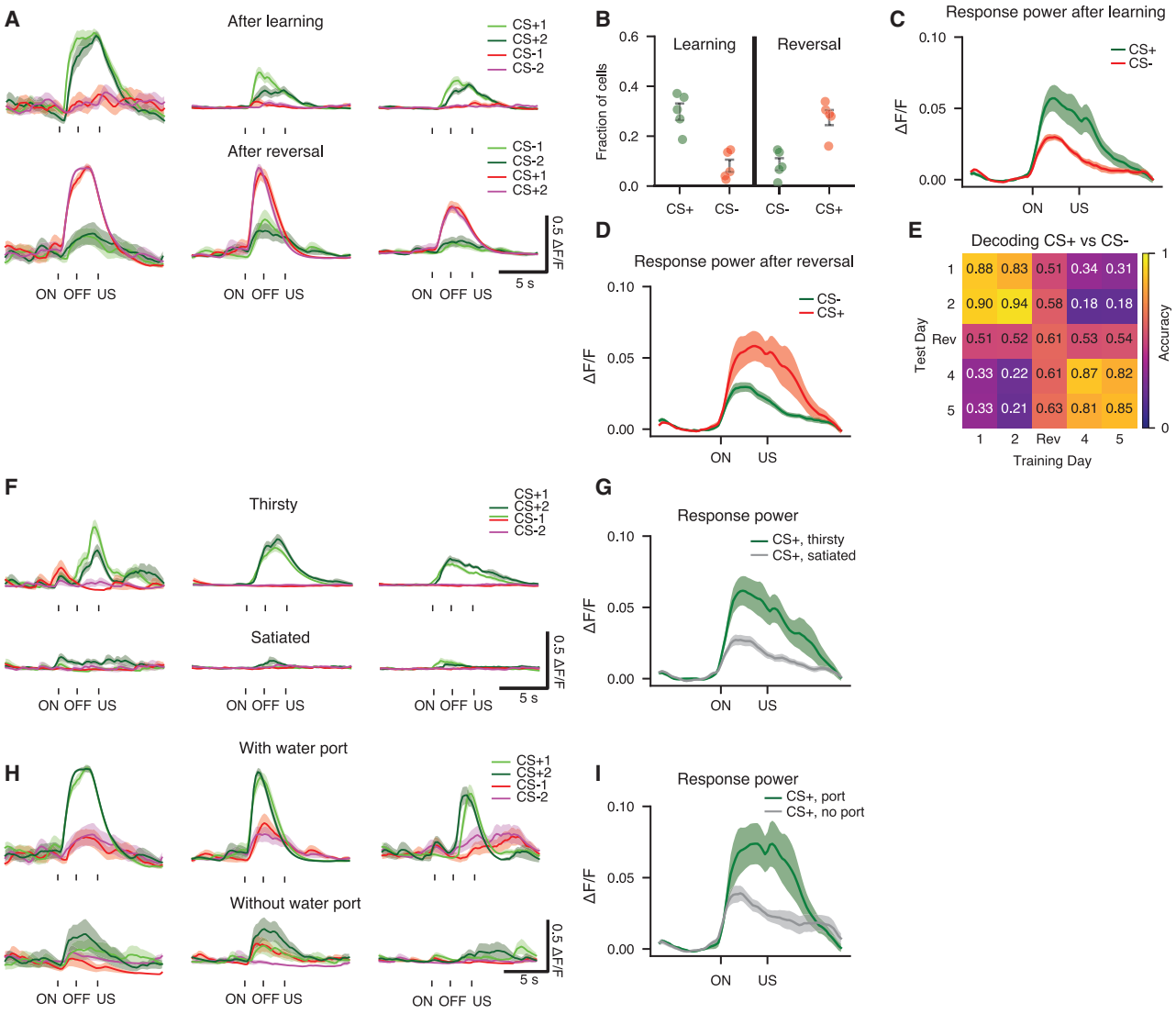

Figure 3. The CS+ Representation in OFC Is Sensitive to Internal State and Task Context

(A) Trial-averaged responses of 3 example OFC cells after learning (top) and after reversal (bottom). Light and dark green odors are rewarded during discrimination learning, but not during reversal. Light and dark red odors are not rewarded during discrimination learning but are rewarded during reversal. Here and below, shading indicates ± 1 SEM.

(B) Fraction of neurons that are more responsive to either CS+ or CS− odors after learning and after reversal for 5 mice. Error bars indicate mean ± 1 SEM. See STAR Methods. Here and below, see Table S1 for values.

(C and D) Average excitatory response power of OFC neurons to CS+ and CS− odors after learning (C) and after reversal (D). n = 5 mice.

(E) Accuracy of decoding predictive value (CS+ odors versus CS− odors) from OFC population activity within and across training days during learning and reversal. Chance accuracy is 0.5.

(F) Trial-averaged responses of 3 example OFC cells in an animal that is thirsty (top) and then immediately satiated (bottom).

(G) Average excitatory response power of the OFC population to CS+ odors in thirsty mice (green) and satiated mice (gray). n = 5 mice.

(H) Trial-averaged responses of 3 example cells when the lick port is present (top) or absent (bottom).

(I) Average excitatory response power of the OFC population to CS+ odor when the lick port is present (green) or absent (gray). n = 4 mice.

See also Figure S5.

odors (CS+ upon reversal) and suppressed anticipatory licking in response to the old CS+ odors (CS− upon reversal) after 20 trials (Figure S5A). Before reversal, imaging revealed that 30% of the neurons were more responsive to CS+ than to CS− odors (Figure 3B; STAR★ Methods). After reversal learning, 91% of the neurons responsive to CS+ odors diminished their response to the old CS+ odors. 68% of these neurons were now activated by the new CS+ odors (Figures S5B and S5C). We also analyzed the strength of the odor-evoked responses during reversal learning at the level of neuronal populations. The response power to the old CS+ odors diminished by 45% upon reversal (Figures 3C and 3D, green; $p < 0.01$), whereas the response power to the old CS−

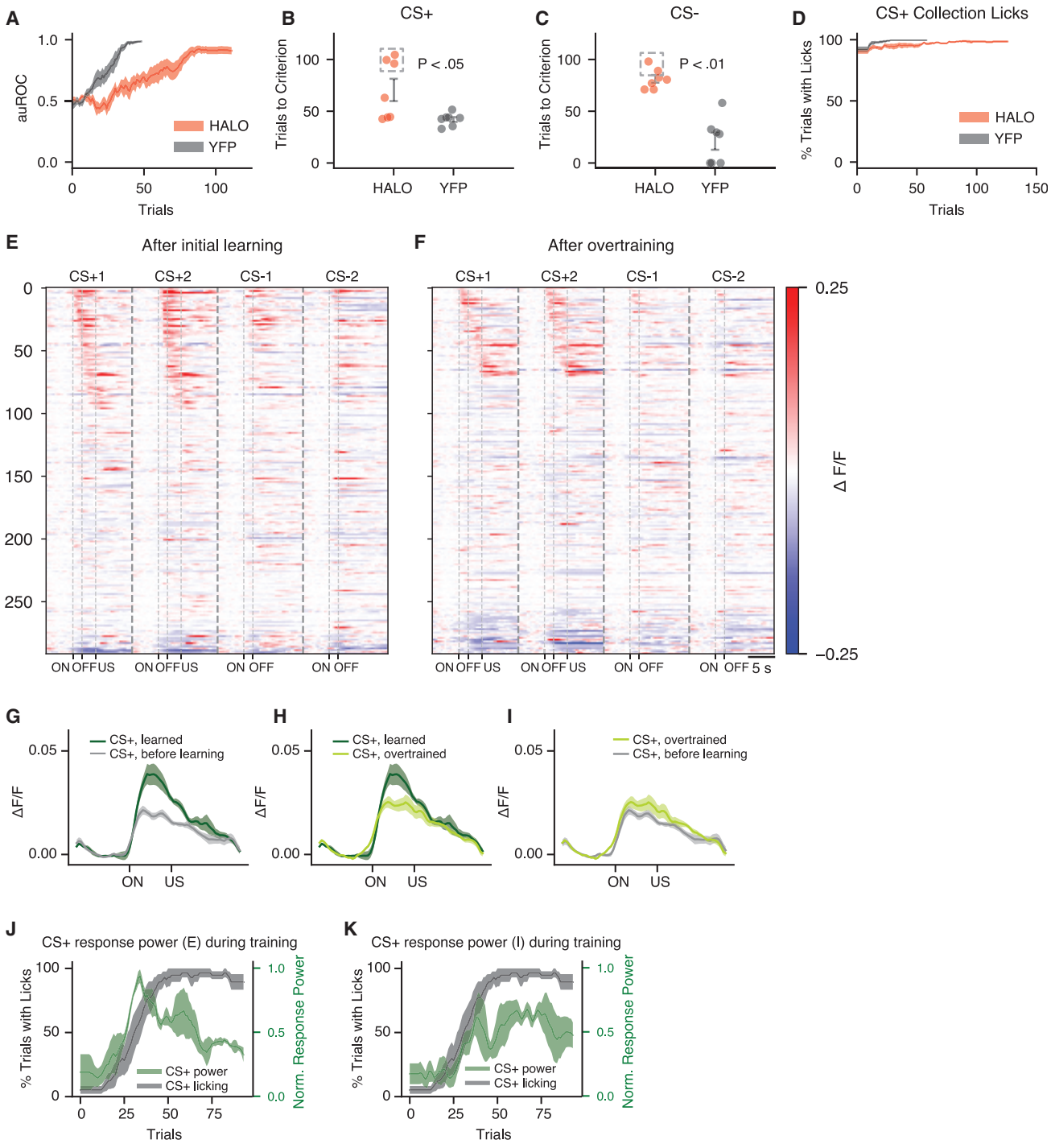

Figure 4. OFC Is Necessary for Associative Learning, and the Odor Representation in OFC Peaks during Learning but Diminishes after Learning

(A–D) Appetitive learning with optogenetic silencing of OFC. Red, inhibited; gray, YFP controls. (A) Discriminability of anticipatory licking in response to CS+ and CS− odors. An AUC (area under ROC curve) of 0.5 indicates zero discriminability between licks to CS+ and CS− odors; an AUC of 1.0 indicates complete discriminability. Here and below, shading indicates ± 1 SEM. (B and C) Summary of trials to the criterion for licking in response to CS+ odors (B) and for suppression of licking in response to CS− odors (C). 3 inhibited mice in (B) and 2 inhibited mice in (C) did not reach the criterion at the end of training (dotted square). Trials to the criterion for these mice were defined as the last trial of training. Here and below, dots represent individual animals and error bars indicate mean ± 1 SEM. See Table S1 for values. (D) Percentage of trials with collection licks to CS+ odors.

(legend continued on next page)

odors increased by 84% upon reversal (Figures 3C and 3D, red; $p < 0.05$). In accordance with these observations, a decoder trained on population responses before reversal classified the old CS+ odors as CS− and the old CS− odors as CS+ after reversal (Figure 3E). Moreover, the accuracy of decoding CS+ or CS− identity was close to chance levels across reversal learning (Figures S5D and S5E). The observation that after reversal the same cells diminished their responses to the old CS+ odors and responded to the new CS+ odors indicates that OFC neurons encode value rather than odor identity.

The value of a sensory stimulus in our appetitive conditioning task should be contingent on the animal's state of satiety (internal state) and the presence or absence of the reward port (context) (Allen et al., 2019; Critchley and Rolls, 1996). CS+ odors predict water reward, an outcome of value to a thirsty mouse but of diminished value to a water-sated mouse. We therefore asked whether the representation of CS+ odors in OFC differs in thirsty and satiated mice. After appetitive learning, the mice were provided water. After satiation, the mice no longer displayed anticipatory licking in response to CS+ odors and rarely collected water when it was delivered (licking in less than 10% of trials) (Figure S5F). Imaging in the OFC revealed that before satiation, 29% of neurons responded to CS+, but 95% of these neurons were either unresponsive or responses were significantly attenuated after satiation (Figures S5G and S5H). At a population level, the response power to the CS+ odors was 2-fold higher (206%) in thirsty mice (Figure 3G; $p < 0.01$).

We also imaged mice in which the behavioral context was altered by removal of the water port. Under these conditions, water is not obtainable, and the value of the CS+ odor is presumably eliminated. Removal of the water port suppressed anticipatory licking in response to CS+ odors in less than three odor presentations (video recordings during imaging). Neuronal responses to the CS+ odors were either eliminated or significantly attenuated in 81% of the neurons responsive to CS+ (Figures 3H, 3I, S5I, and S5J). The response power to the CS+ odors was 2-fold higher (195%, $p < 0.05$) before water port removal (Figure 3I). Thus, changes in internal state and task context that diminished the value of water reward correlated with a significant attenuation in the activity of the CS+ ensemble, providing further evidence that this OFC representation encodes value.

The Role of the OFC Representation in Associative Learning

We next performed optogenetic silencing to ask whether the OFC contributes to the learning of appetitive associations. AAV (adeno-associated virus) encoding either halorhodopsin (AAV5-hSyn-eNPHR3.0-EYFP) or YFP (AAV5-hSyn-EYFP) was injected bilaterally into OFC (Gradinaru et al., 2008). Electrophysiological recording using a 32-channel extracellular optrode array (Royer et al., 2010) demonstrated that photostimulation results in more than an 8-fold decrease in the average firing rate in mice expressing halorhodopsin (Figures S6A and S6B). Silencing of OFC during training was initiated 2 s before odor delivery and extended for 2 s beyond the delivery of the US (see Figure 1A for trial structure). Mice that experienced OFC inhibition exhibited significant learning deficits (Figures 4A–4D). Silenced mice ($n = 7$) did not lick consistently in response to the CS+ odors, licked indiscriminately to CS+ and CS− odors, or both (Figure 4A). The number of trials required to learn to lick to CS+ odors (anticipatory licking in more than 80% of CS+ odor trials) was almost two-fold higher in OFC-silenced mice than in control mice injected with YFP (Figure 4B; Halo [halorhodopsin]: 71; YFP: 42, $p < 0.05$). In addition, the number of trials required to learn to suppress licking in response to CS− odors (anticipatory licking in less than 20% of CS− odor trials) was almost four-fold higher in OFC-silenced mice than in control mice (Figure 4C; Halo: 81; YFP: 21, $p < 0.01$). Moreover, 5 of 7 mice failed to discriminate between CS+ and CS− odors even after 100 presentations of each odor (Figures 4B and 4C, gray squares). Both control and silenced mice exhibited robust licking upon delivery of the US in CS+ trials, suggesting that mice with OFC inhibition were highly motivated to acquire water reward (Figure 4D). Thus, the neural representation of predictive value in OFC participates in the efficient acquisition of appetitive associations.

CS+ Responses in OFC Diminish after Learning

CS+ responses in OFC were strongest after 3 to 4 days of training, corresponding to the plateau in behavioral performance (Figure 2D). We performed imaging experiments in a new cohort of mice for longer periods extending up to 9 training days and observed that the CS+ responses diminished at later times despite the persistence of learned behavior (Figures 4E and 4F). The excitatory response power of the CS+ representation was maximal at 3 to 4 days of training for each mouse and steadily declined to amplitudes observed before training after 6–9 training days (Figures 4G–4J; power before versus after learning: $p < 0.05$; power after learning versus after overtraining: $p < 0.05$, Wilcoxon signed-rank test). This decrease in response power is not the consequence of changes in inhibitory responses, which were variable and did not appear to diminish or increase consistently during prolonged training (Figure 4K). The observation that excitatory responses to CS+ odors in the OFC diminished, whereas the behavioral accuracy persisted, suggests that OFC may participate in the acquisition of appetitive associations but is no longer required after initial learning.

Phases of Olfactory Learning

Our olfactory association task may involve distinct phases of learning with only the initial phase dependent on OFC. One possibility is that mice first learn that odor predicts water and then, in

(E and F) PSTHs of OFC responses for all mice ($n = 3$) to CS+ and CS− odors after initial learning (E, days 3–4 of training) and after overtraining (F, days 8–9 of training). Responses are sorted independently by response onset to CS+ odors.
(G–I) Average excitatory response power of OFC neurons to CS+ odors (G) before learning (gray) and after learning (dark green, $n = 3$ mice), (H) after learning (dark green) and after overtraining (light green, $n = 3$ mice), and (I) before learning (gray) and after overtraining (light green, $n = 3$ mice).
(J and K) Excitatory (J) and inhibitory (K) response power of OFC neurons to CS+ odors (green) versus percentage of CS+ trials with anticipatory licks (gray).
See also Figure S6.

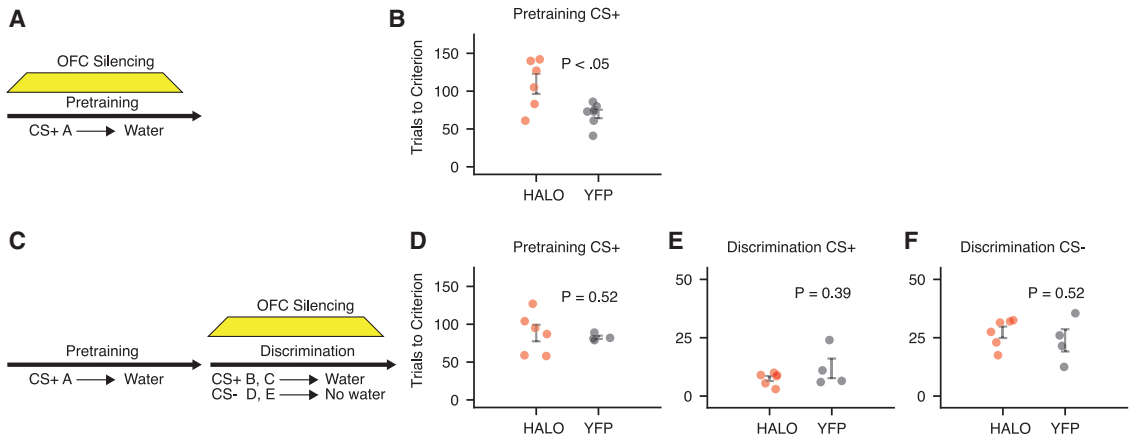

Figure 5. OFC Is Necessary for Initial Learning

(A and C) Schematic of optogenetic silencing of OFC (A) during pretraining and (C) during discrimination in the two-phase, head-fixed task. Different animal cohorts were used in the two silencing experiments.

(B, D, E, and F) Trials to the criterion for (B) licking in response to the pretraining odor with OFC silencing, (D) licking in response to the pretraining odor without OFC silencing, (E) licking in response to the CS+ odors during discrimination training, and (F) suppression of licking in response to the CS− odors during discrimination training. See Table S1 for values.

See also Figure S6.

a second phase of learning, acquire the ability to discriminate between CS+ and CS− odors. We therefore implemented a head-fixed associative learning task consisting of two phases: pretraining and discrimination (Figures 5A and 5C). This task is similar to learning paradigms in freely moving mice that require pretraining for task acquisition, but the role of specific brain regions in pretraining in these behavioral experiments has not been examined. In the pretraining phase of our new task, a single odor was paired with the US. After mice successfully learned that odor predicts reward, a discrimination phase was initiated in which two new CS+ and two CS− odors were presented. This two-phase learning paradigm was conducted in mice expressing either AAV5-hSyn-eNPHR3.0-EYFP or AAV5-hSyn-EYFP in all neurons in the OFC. OFC silencing impaired learning in the pretraining phase, with anticipatory licking requiring an average of 110 trials compared with 70 trials in control mice (Figures 5A and 5B; $p < 0.05$, rank-sum test).

We next examined the role of OFC during discrimination in the two-phase, odor-learning task. Mice expressing either halorhodopsin or YFP in the OFC were pretrained in the absence of inhibition. After mice successfully learned that odor predicts reward, anticipatory licking was observed in response to both CS+ and CS− odors at the start of discrimination (Figures S6F and S6G). This behavior contrasts with the absence of anticipatory licking observed in response to the CS+ odor at the start of pretraining (Figure S6E). This suggests that during pretraining with a single CS+ odor, mice learned to generalize, associating all odors with reward. Photoillumination of the OFC during the discrimination phase in mice expressing halorhodopsin did not impair discrimination learning. Licking in response to CS+ odors (Figure 5E; Halo trials: 8; YFP trials: 12, $p = 0.39$, rank-sum test) and suppression of licking in response to CS− odors (Figure 5F; Halo trials: 27; YFP trials: 24, $p = 0.52$) were similar in silenced and control mice.

We also examined the role of the OFC in a two-phase, freely moving behavioral paradigm (Figures S6K–S6T). In this task, freely moving mice first learned an association between odor and water and then learned to discriminate between new CS+ and CS− odors. The results of OFC inhibition in freely moving mice are in accordance with our observations in the head-fixed paradigm. These data suggest that during the pretraining phase, mice learn a simple association between odor and reward and this learning is impaired upon silencing of the OFC. Once the association is learned, the OFC is no longer required and a second brain structure facilitates the subsequent learning necessary for discrimination.

The Representation of Value in OFC in the Two-Phase Paradigm

We performed imaging experiments to examine the relationship between odor representations in OFC and behavior in the two-phase, head-fixed task (Figure S7A). During pretraining, a strong CS+ representation emerges, with 26% (±5% SEM for individual mice) of the neurons responding to the pretraining CS+ odor (Figure 6A). The response power to the CS+ odor increased 2-fold (183%) after learning (Figure 6E; $p = 0.068$). We then performed imaging during discrimination training, with mice exposed to two new CS+ and two CS− odors. At the start of discrimination, the responses to each of the four odors were non-selective and weak in amplitude (Figures 6B, 6F, and 6I). During discrimination training, neurons became selectively responsive to the CS+ odors (Figure 6C). Decoding analysis revealed that before discrimination learning, the CS+ and CS− ensembles were not well separated (Figure 6L; accuracy: 68%). After learning, the decoding accuracy increased to 94% (Figure 6L; $p = 0.067$). The amplitude of the response to the CS+ odors after discrimination learning was lower than the response to the pretraining CS+ odor after learning (power increase: after pretraining, 183%; after discrimination learning, 139%, $p < 0.05$). We continued to image the OFC for

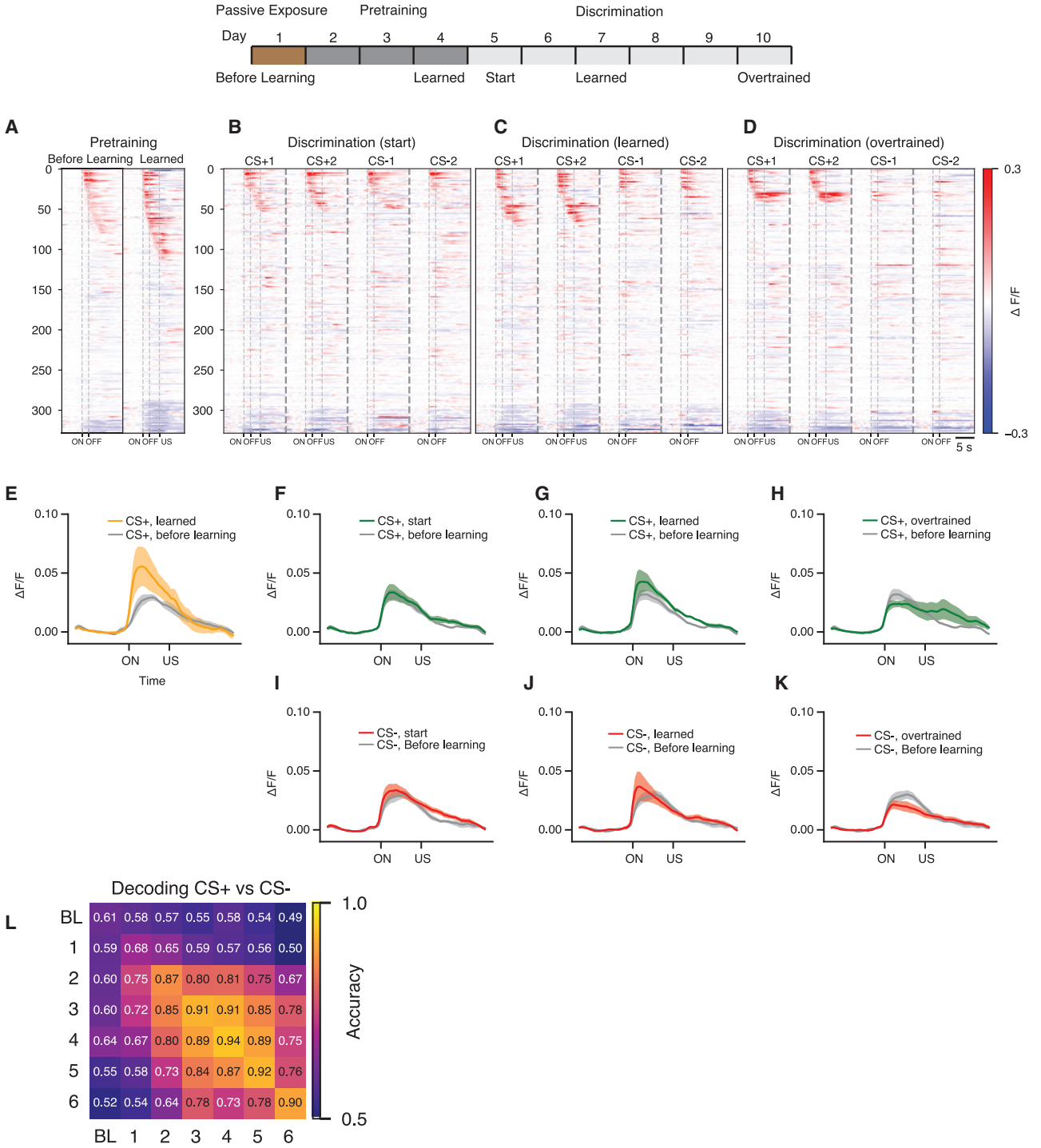

Figure 6. The Odor Representation in OFC Peaks during Pretraining and Diminishes during Discrimination Learning

Top, schematic of the training sequence in the two-phase task, indicating the training epochs for which imaging data are shown below.

(A–D) PSTH of OFC responses during multiple days of the two-phase task in all animals (n = 4). Responses on different days are sorted independently. (A) Responses to the CS+ odor during the pretraining phase before and after learning. (B–D) Responses to 2 new CS+ and 2 CS− odors on the first day of discrimination training (B), after complete discrimination learning (C), and after overtraining (D).

(E) Response power of the OFC representation to the CS+ odor before pretraining (gray) and after pretraining (orange). Here and below, shading indicates ± 1 SEM. See Table S1 for values.

(F–H) CS+ response power on the first day of discrimination learning (F), after discrimination learning (G), and after overtraining (H). Green, CS+ odors after learning; gray, CS+ odors before learning.

(legend continued on next page)

up to 4 days after discrimination learning plateaued. CS+ responses in OFC gradually diminished (Figures 6D and S7A), and the response power decreased below the response to odors before training (Figure 6H; 8% decrease in power, $p < 0.05$). These imaging results are consistent with the behavioral observations: OFC is required to learn the association of the pretraining odor with water, and a strong representation of this odor is observed upon imaging. After pretraining, OFC is not required for discrimination, and a weaker CS+ representation emerges during this phase of the task. These results suggest that a second brain structure is employed to accomplish the task of discrimination learning.

A Representation of Value in the mPFC

Previous experiments have implicated the mPFC in reward learning (Birrell and Brown, 2000; Chudasama and Robbins, 2003; Kim et al., 2017; Kitamura et al., 2017; Ostlund and Balleine, 2005; Otis et al., 2017). We therefore performed imaging in the mPFC to discern whether a representation of value emerges during discrimination learning in the two-phase task that may support learning after the diminution of the OFC representation (Figure S7B). Imaging of the mPFC during pretraining revealed that the responses to the pretraining odor were sparse and of low amplitude and did not increase significantly with learning (Figures 7A and 7E; 20% increase, $p = 0.27$). Mice were then exposed to two new CS+ and two CS− odors. At the start of discrimination training, we observed neural responses to all odors (Figures 7B, 7F, and 7I). The population activities evoked by these odors were more correlated (Figures 7L and 7M; correlation before training: 0.39; start of discrimination: 0.56, $p < 0.001$) and of higher amplitude (Figures 7F and 7I) than before training and may reflect generalized licking in response to all odors (Figures S6F and S6G).

As learning proceeded, we observed a population of neurons responsive only to CS+ odors (Figure 7C; before learning: 10%; after learning, 19%, $p < 0.05$), accompanied by a second population responsive to CS− odors (Figure 7C; before learning: 12%; after learning: 22%, $p < 0.05$). The CS+ and CS− representations increased in amplitude (Figures 7G and 7J) and became more separable during discrimination learning (Figure 7N; correlation between CS+ versus CS− at start of discrimination learning, 0.52; after learning, 0.24, $p < 0.05$). We continued to image the mPFC for up to 4 days after learning plateaued, and unlike the OFC representations, the mPFC ensembles remained strong and stable (Figures 7D, 7H, and 7K). After prolonged training, 23% of mPFC neurons responded to CS+ odors (Figure 7D), and a non-overlapping 25% of mPFC neurons responded to CS− odors (Figures 7D and 7O). These results are supported by decoding analysis that revealed that the representations of CS+ and CS− odors were stable and separable after discrimination learning (Figure 7P; 95% accuracy).

Thus, in mPFC, we observed robust responses to CS+ and CS− odors during discrimination learning but did not observe a response to the CS+ odor during pretraining. The mPFC therefore appears to transform a representation of odor identity encoded in piriform into two distinct and stable representations: a CS+ ensemble encoding positive value and a CS− ensemble encoding negative value.

The Role of the mPFC in Associative Learning

The emergence of CS+ and CS− representations in mPFC during discrimination coincided with the observed behavioral distinction between CS+ and CS− odors. We therefore examined the role of mPFC in the two-phase behavioral paradigm. Mice expressing either halorhodopsin or YFP in the mPFC were photoilluminated during the different phases of the task. Inactivation of the mPFC during pretraining did not inhibit task performance (Figure 7Q; trials to the criterion: Halo, 76; YFP, 75, $p = 1.0$), whereas silencing during discrimination impaired appetitive learning. During the discrimination phase, control mice expressing YFP learned to lick in response to the CS+ odors in an average of 6 trials, but upon silencing, in mice expressing halorhodopsin, an average of 16 trials were required to reach criterion (Figure 7S; $p < 0.05$). A similar impairment is observed in the suppression of licking in response to CS− odors upon silencing of mPFC. Suppression of licking occured in an average of 5 trials in control, whereas mice expressing halorhodopsin required an average of 25 trials (Figure 7T; $p < 0.01$). Similar results were observed when the mPFC was inhibited in the freely moving task (Figures S7C–S7F). Inactivation of the mPFC during pretraining in freely moving mice did not impair learning (Figure S7C; Halo trials: 250; YFP trials: 225, $p = 0.52$), whereas silencing during discrimination impaired anticipatory licking in response to CS+ odors (Figure S7E; Halo trials: 77; YFP trials: 11, $p < 0.01$).

These data suggest that the neural representation in OFC during pretraining contributes to the learning of an association between odor and water. CS+ responses in OFC diminished upon discrimination learning, and a persistent representation of both CS+ and CS− odors emerged in the mPFC. The mPFC participates in the discrimination of odors predictive of reward, suggesting a transfer of information from OFC to mPFC in odor learning.

DISCUSSION

Representation of Odor Identity in Piriform Cortex

A representation of odor identity in piriform is largely unaltered upon olfactory conditioning. Rather, a representation of value emerges transiently in OFC and stably in mPFC. The imposition of value downstream of piriform may be important to preserve odor identity while allowing flexible behavioral output (Choi et al., 2011). Imposing value in piriform would result in the modification of outputs to all of piriform's downstream targets, which could drive conflicting behavioral outputs. In addition, if value

(I–K) CS− response power on the first day of discrimination learning (I), after discrimination learning (J), and after overtraining (K). Red, CS− odors after learning; gray, CS− odors before learning.

(L) Accuracy of decoding predictive value (CS+ odors versus CS− odors) from OFC population activity within and across training days (n = 4 mice).

See also Figure S7A.

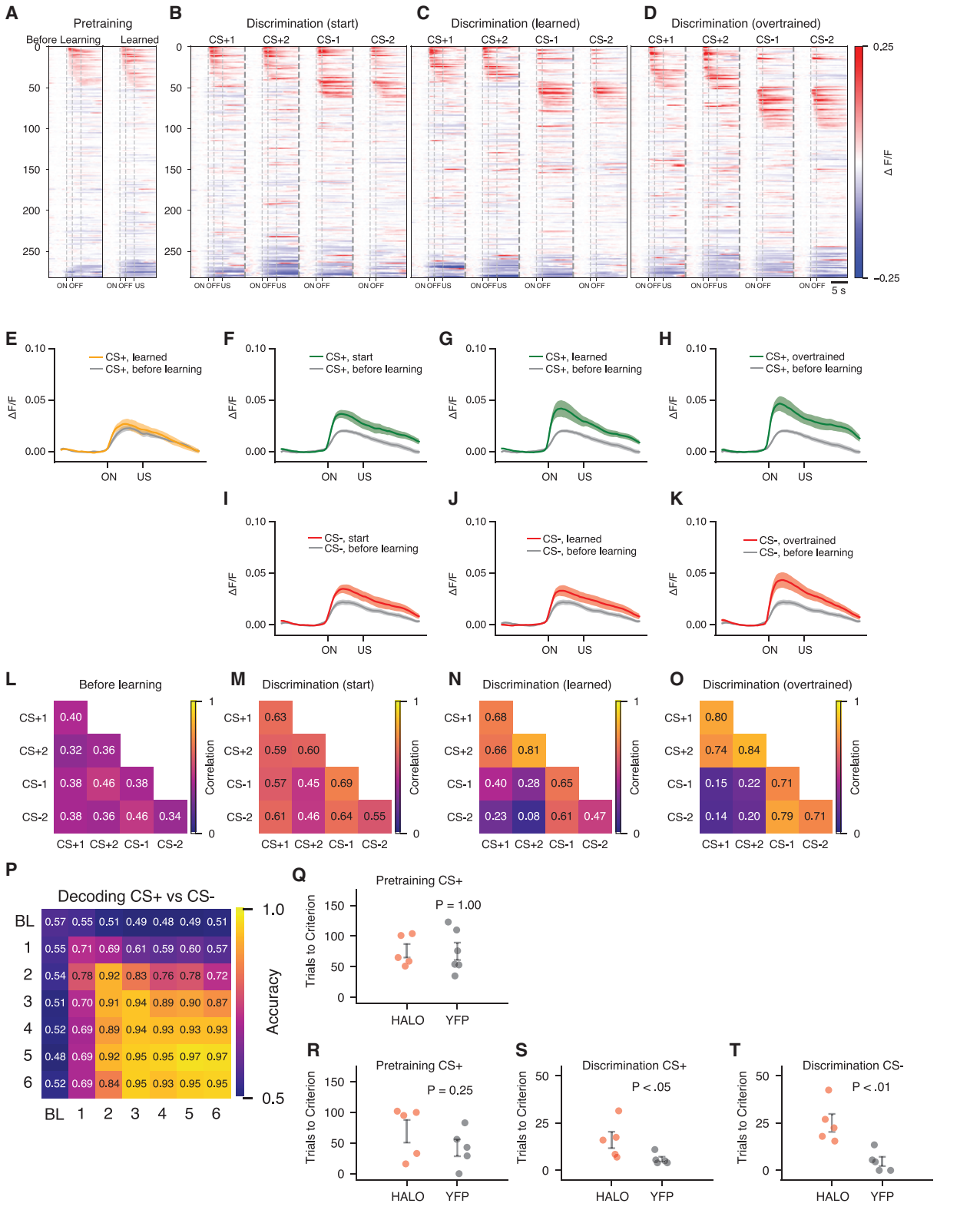

(legend on next page)

were imposed in piriform cortex, gating by internal state or by task context in piriform would limit the perception of odor to subsets of states and contexts. Finally, changes in the weights of either bulbar inputs or associative connections between pyramidal neurons reflective of value could reduce the dimensionality of the odor representation in piriform. Thus, the imposition of value in downstream areas allows the piriform to maintain a high-dimensional representation of odor information that can support flexible and specific associations in multiple downstream regions.

Representations of Value in OFC and mPFC

We observed a representation of odor identity in piriform and representations of CS+ odors in OFC, and both CS+ and CS− odors in mPFC. Representations of conditioned stimuli have been described in multiple brain regions during an associative learning task similar to our behavioral paradigm (Allen et al., 2019; Kim et al., 2017; Namboodiri et al., 2019; Otis et al., 2017). A neural representation of rewarded auditory stimuli was identified in the OFC that is necessary for learning. These neurons exhibited heterogeneity in their response patterns, but a significant fraction were modulated by reward value. Imaging of the mPFC during this behavioral paradigm revealed a population of CS+ neurons, but CS− representation was not observed after learning. The structure of the behavioral task and lens placement may explain these differences.

We have implemented an associative learning task consisting of two phases, pretraining and discrimination, to understand the contributions of OFC and mPFC to learning. Our data suggest that during pretraining, mice learn a simple association between odor and reward that engages a representation of value in OFC. Once this association is learned, OFC is no longer required for subsequent odor discrimination; the representation in mPFC then facilitates the learning of associations necessary for discrimination.

Previous studies have concluded that lesions of OFC do not impair learning of appetitive associations (Burke et al., 2008; Chudasama and Robbins, 2003; Gallagher et al., 1999; Izquierdo et al., 2004; Ostlund and Balleine, 2007; Schoenbaum et al., 2002; Stalnaker et al., 2007). These studies also employed a two-phase conditioning task, but the consequence of lesioning of OFC during pretraining was not assessed. Similar to our observations, lesioning of OFC did not impair discrimination after animals were pretrained. A recent study that used a one-phase task observed that OFC inhibition impairs acquisition of learning, in agreement with our results (Namboodiri et al., 2019). Our studies associate different brain regions with the two phases of the task, pretraining and discrimination, and reveal the importance of OFC in the formation specific of associations between stimulus and reward during initial task learning.

Representations of Value in Multiple Brain Regions

Our data suggest that odor learning reinforces piriform inputs to OFC, activating a representation of value. OFC may then teach mPFC during discrimination by reinforcing piriform inputs to this brain structure. In this manner, parallel inputs from piriform to multiple downstream targets can be sequentially reinforced to generate multiple representations of odor value.

The observation that the OFC representation precedes that of the mPFC suggests the transfer of information from OFC to mPFC. Contextual fear memory is also thought to require the transfer and consolidation of information. A salient context is initially thought to elicit a representation in CA1 of the hippocampus, which over time reinforces a contextual representation in mPFC (Bontempi et al., 1999; Goshen et al., 2011; Kim and Fanselow, 1992; Kitamura et al., 2017; Squire and Alvarez, 1995; Takehara-Nishiuchi and McNaughton, 2008). At early times after learning, behavior depends on temporal lobe structures. However, remote recall depends on mPFC and no longer requires an active hippocampus. The persistence of remote contextual memories after bilateral hippocampal ablations argues for consolidation in cortex dependent upon a reinforcing teaching function mediated by the hippocampus.

Theoretical considerations also reveal advantages to encoding memories in multiple, partitioned brain structures (McClelland et al., 1995; Roxin and Fusi, 2013). The persistence of individual representations depends on the stability of synaptic reinforcement in different brain regions and may dictate their role in the learning process. Plastic synapses effecting fast learning

Figure 7. CS+ and CS– Representations Emerge in mPFC during Discrimination, and mPFC Is Required for Discrimination Learning

(A–D) PSTH of mPFC responses during multiple days of the two-phase task in all animals (n = 4). Responses on different days are sorted independently. (A) Responses to the CS+ odor during the pretraining phase before and after learning. (B–D) Responses to 2 new CS+ and 2 CS− odors on the first day of discrimination training (B), after discrimination learning (C), and after overtraining (D).

(E) CS+ response power before pretraining (gray) and after pretraining (orange). Here and below, shading indicates ± 1 SEM for control animals. See Table S1 for values.

(F–H) CS+ response power on the first day of discrimination learning (F), after discrimination learning (G), and after overtraining (H). Green, CS+ odors after learning; gray, CS+ odors before learning.

(I–K) CS− response power on the first day of discrimination learning (I), after discrimination learning (J), and after overtraining (K). Red, CS− odors after learning; gray, CS− odors before learning.

(L–O) Within-day correlations between population activities for all pairs of odors before training (L), during the first day of discrimination training (M), after discrimination learning (N), and after overtraining (O).

(P) Accuracy of decoding of the predictive value (CS+ odors versus CS− odors) from mPFC population activity within and across training days (n = 4 mice). Chance accuracy is 0.5.

(Q) mPFC silencing during the pretraining phase of the two-phase task in head-fixed animals. Trials to the criterion for licking in response to the pretraining CS+ odor. Here and below, error bars indicate mean ± 1 SEM.

(R–T) mPFC inhibition during the discrimination phase of the two-phase task in head-fixed animals. Trials to the criterion for (R) licking in response to the pretraining CS+ odor, (S) licking in response to the CS+ odors during discrimination training, and (T) suppression of licking in response to the CS− odors during discrimination training.

See also Figure S7.

can be rapidly overwritten, whereas less plastic synapses in different brain structures can stabilize memories (Benna and Fusi, 2016; Fusi et al., 2005; Roxin and Fusi, 2013). Whatever the advantage afforded by an early OFC representation, it must be transient, because the responses of value-encoding neurons dissipate while the mPFC representation remains stable. The transient nature of the OFC population supports models in which OFC performs a teaching function during task acquisition, after which it is no longer required for learning discrimination or for the expression of the learned behavior.

The OFC Representation Depends on State and Context

The piriform cortex represents the external world, the identity of an odor, whereas OFC and mPFC represent not only the external sensory world but also internal features: learning, context, and state. This representation of value in OFC depends on the coincidence of a conditioned stimulus, motivated internal state and appropriate context, and undoubtedly other factors that we have not explored. One simple model that incorporates these features invokes direct input of piriform neurons onto pyramidal cells in OFC. OFC neurons may also receive inhibitory inputs that prevent the animal from seeking water when the animal is satiated, and these inhibitory inputs may be disinhibited when the animal is in a thirsty state and in the appropriate context. This model affords flexibility whereby the same neurons in OFC can represent input from multiple sensory modalities, encoding value and gated by different states or contexts.

The Generation of Distinct CS+ and CS– Representations

How do representations of CS− and CS+ odors arise in distinct populations of cells in the mPFC? In one model, during pretraining, animals exposed to a single CS+ may learn that odor predicts reward through the emergence of a CS+ representation in the OFC. This CS+ representation in OFC may serve a teaching function in the mPFC at the initiation of discrimination learning and reinforce all piriform inputs onto the mPFC. Early in discrimination learning, all odors will therefore activate the mPFC CS+ ensemble and drive generalized licking behavior. When the animals experience odors that are not associated with reward (CS−), a negative reward prediction error (RPE) signal may be generated by the failure of these odors to predict reward (Schultz, 2016). This negative RPE signal is then relayed onto the mPFC to drive the formation of a CS− ensemble in the mPFC, distinct from the CS+ ensemble. In this manner, CS− odors will activate a distinct population of neurons in the mPFC that signals a negative value. This model invokes the presence of cognitive representations of odor in at least three brain regions, each contributing a different component function that ultimately leads to stable yet flexible memory of the stimulus value.

STAR★METHODS

Detailed methods are provided in the online version of this paper and include the following:

- KEY RESOURCES TABLE
- RESOURCE AVAILABILITY
  - Lead Contact
  - Materials Availability
  - Data and Code Availability
- EXPERIMENTAL MODEL AND SUBJECT DETAILS
- METHOD DETAILS
  - Stereotaxic Surgeries
  - Animal Behavior
  - Head-fixed Imaging
  - Optrode Experiments
  - Histology
  - RNA-scope
  - Data Collection and Exclusion
- QUANTIFICATION AND STATISTICAL ANALYSIS
  - Behavioral Data Analysis
  - Image Processing
  - Calcium Transient Analysis
  - Quantification of Significant Neuronal Responses
  - Response Power
  - Correlation Analysis
  - Decoding

SUPPLEMENTAL INFORMATION

Supplemental Information can be found online at https://doi.org/10.1016/j.neuron.2020.07.033.

ACKNOWLEDGMENTS

We thank Cory Root, Dan Constantini, Abigail Zadina, and Kristen Lawlor for experimental help; Fabio Stefanini for input on decoding; Walter Fischler, Stefano Fusi, Rui Costa, Robert Sandeep Datta, Daniel Salzman, Ashok Litwin-Kumar, Abbas Rizvi, and members of the Axel and Abbott laboratories for discussions; and Clayton Eccard for assistance in the preparation of the manuscript. This work is supported by the Columbia Neurobiology and Behavior Program (P.Y.W.), the Helen Hay Whitney Foundation (C.B.), the Simons Foundation (L.F.A. and R.A.), NSF NeuroNex award DBI-1707398 and the Gatsby Charitable Foundation (L.F.A.), and the Howard Hughes Medical Institute (R.A.). R.A. is an HHMI investigator.

AUTHOR CONTRIBUTIONS

P.Y.W., C.B., L.F.A., and R.A. conceived the project, participated in its development, and wrote the paper. P.Y.W., C.B., M.C., A.H.-H., and N.P.S. performed the behavioral experiments and optogenetic manipulations. P.Y.W. performed the imaging experiments and data analysis. P.Y.W., Z.W., and P.S. performed optrode experiments.

DECLARATION OF INTERESTS

The authors declare no competing interests.

Received: August 29, 2019
Revised: March 10, 2020
Accepted: July 24, 2020
Published: August 21, 2020

SUPPORTING CITATIONS

The following reference appears in the Supplemental Information: Boulland et al., (2004).

REFERENCES

Allen, W.E., Chen, M.Z., Pichamoorthy, N., Tien, R.H., Pachitariu, M., Luo, L., and Deisseroth, K. (2019). Thirst regulates motivated behavior through modulation of brainwide neural population dynamics. Science *364*, 253.

Bari, B.A., Grossman, C.D., Lubin, E.E., Rajagopalan, A.E., Cressy, J.I., and Cohen, J.Y. (2019). Stable Representations of Decision Variables for Flexible Behavior. Neuron *103*, 922–933.e7.

Barretto, R.P., Messerschmidt, B., and Schnitzer, M.J. (2009). *In vivo* fluorescence imaging with high-resolution microlenses. Nat. Methods *6*, 511–512.

Benna, M.K., and Fusi, S. (2016). Computational principles of synaptic memory consolidation. Nat. Neurosci. *19*, 1697–1706.

Birrell, J.M., and Brown, V.J. (2000). Medial frontal cortex mediates perceptual attentional set shifting in the rat. J. Neurosci. *20*, 4320–4324.

Bissonette, G.B., Martins, G.J., Franz, T.M., Harper, E.S., Schoenbaum, G., and Powell, E.M. (2008). Double dissociation of the effects of medial and orbital prefrontal cortical lesions on attentional and affective shifts in mice. J. Neurosci. *28*, 11124–11130.

Bontempi, B., Laurent-Demir, C., Destrade, C., and Jaffard, R. (1999). Time-dependent reorganization of brain circuitry underlying long-term memory storage. Nature *400*, 671–675.

Boulland, J.L., Qureshi, T., Seal, R.P., Rafiki, A., Gundersen, V., Bergersen, L.H., Fremeau, R.T., Jr., Edwards, R.H., Storm-Mathisen, J., and Chaudhry, F.A. (2004). Expression of the vesicular glutamate transporters during development indicates the widespread corelease of multiple neurotransmitters. J. Comp. Neurol. *480*, 264–280.

Buck, L., and Axel, R. (1991). A novel multigene family may encode odorant receptors: a molecular basis for odor recognition. Cell *65*, 175–187.

Burke, K.A., Franz, T.M., Miller, D.N., and Schoenbaum, G. (2008). The role of the orbitofrontal cortex in the pursuit of happiness and more specific rewards. Nature *454*, 340–344.

Calu, D.J., Roesch, M.R., Stalnaker, T.A., and Schoenbaum, G. (2007). Associative encoding in posterior piriform cortex during odor discrimination and reversal learning. Cereb. Cortex *17*, 1342–1349.

Chen, T.W., Wardill, T.J., Sun, Y., Pulver, S.R., Renninger, S.L., Baohan, A., Schreiter, E.R., Kerr, R.A., Orger, M.B., Jayaraman, V., et al. (2013). Ultrasensitive fluorescent proteins for imaging neuronal activity. Nature *499*, 295–300.

Chen, C.F., Zou, D.J., Altomare, C.G., Xu, L., Greer, C.A., and Firestein, S.J. (2014). Nonsensory target-dependent organization of piriform cortex. Proc. Natl. Acad. Sci. USA *111*, 16931–16936.

Choi, G.B., Stettler, D.D., Kallman, B.R., Bhaskar, S.T., Fleischmann, A., and Axel, R. (2011). Driving opposing behaviors with ensembles of piriform neurons. Cell *146*, 1004–1015.

Chudasama, Y., and Robbins, T.W. (2003). Dissociable contributions of the orbitofrontal and infralimbic cortex to pavlovian autoshaping and discrimination reversal learning: further evidence for the functional heterogeneity of the rodent frontal cortex. J. Neurosci. *23*, 8771–8780.

Critchley, H.D., and Rolls, E.T. (1996). Hunger and satiety modify the responses of olfactory and visual neurons in the primate orbitofrontal cortex. J. Neurophysiol. *75*, 1673–1686.

Davison, I.G., and Ehlers, M.D. (2011). Neural circuit mechanisms for pattern detection and feature combination in olfactory cortex. Neuron *70*, 82–94.

Denk, W., Strickler, J.H., and Webb, W.W. (1990). Two-photon laser scanning fluorescence microscopy. Science *248*, 73–76.

Diodato, A., Ruinart de Brimont, M., Yim, Y.S., Derian, N., Perrin, S., Pouch, J., Klatzmann, D., Garel, S., Choi, G.B., and Fleischmann, A. (2016). Molecular signatures of neural connectivity in the olfactory cortex. Nat. Commun. *7*, 12238.

Feierstein, C.E., Quirk, M.C., Uchida, N., Sosulski, D.L., and Mainen, Z.F. (2006). Representation of spatial goals in rat orbitofrontal cortex. Neuron *51*, 495–507.

Ferenczi, E.A., Zalocusky, K.A., Liston, C., Grosenick, L., Warden, M.R., Amatya, D., Katovich, K., Mehta, H., Patenaude, B., Ramakrishnan, C., et al. (2016). Prefrontal cortical regulation of brainwide circuit dynamics and reward-related behavior. Science *351*, aac9698.

Fusi, S., Drew, P.J., and Abbott, L.F. (2005). Cascade models of synaptically stored memories. Neuron *45*, 599–611.

Gallagher, M., McMahan, R.W., and Schoenbaum, G. (1999). Orbitofrontal cortex and representation of incentive value in associative learning. J. Neurosci. *19*, 6610–6614.

Ghosh, S., Larson, S.D., Hefzi, H., Marnoy, Z., Cutforth, T., Dokka, K., and Baldwin, K.K. (2011). Sensory maps in the olfactory cortex defined by long-range viral tracing of single neurons. Nature *472*, 217–220.

Godfrey, P.A., Malnic, B., and Buck, L.B. (2004). The mouse olfactory receptor gene family. Proc. Natl. Acad. Sci. USA *101*, 2156–2161.

Goshen, I., Brodsky, M., Prakash, R., Wallace, J., Gradinaru, V., Ramakrishnan, C., and Deisseroth, K. (2011). Dynamics of retrieval strategies for remote memories. Cell *147*, 678–689.

Gottfried, J.A., O'Doherty, J., and Dolan, R.J. (2003). Encoding predictive reward value in human amygdala and orbitofrontal cortex. Science *301*, 1104–1107.

Gradinaru, V., Thompson, K.R., and Deisseroth, K. (2008). eNpHR: a Natronomonas halorhodopsin enhanced for optogenetic applications. Brain Cell Biol. *36*, 129–139.

Guizar-Sicairos, M., Thurman, S.T., and Fienup, J.R. (2008). Efficient subpixel image registration algorithms. Opt. Lett. *33*, 156–158.

Hirokawa, J., Vaughan, A., Masset, P., Ott, T., and Kepecs, A. (2019). Frontal cortex neuron types categorically encode single decision variables. Nature *576*, 446–451.

Illig, K.R., and Haberly, L.B. (2003). Odor-evoked activity is spatially distributed in piriform cortex. J. Comp. Neurol. *457*, 361–373.

Iurilli, G., and Datta, S.R. (2017). Population Coding in an Innately Relevant Olfactory Area. Neuron *93*, 1180–1197.e7.

Izquierdo, A., Suda, R.K., and Murray, E.A. (2004). Bilateral orbital prefrontal cortex lesions in rhesus monkeys disrupt choices guided by both reward value and reward contingency. J. Neurosci. *24*, 7540–7548.

Johnson, D.M., Illig, K.R., Behan, M., and Haberly, L.B. (2000). New features of connectivity in piriform cortex visualized by intracellular injection of pyramidal cells suggest that "primary" olfactory cortex functions like "association" cortex in other sensory systems. J. Neurosci. *20*, 6974–6982.

Jung, J.C., Mehta, A.D., Aksay, E., Stepnoski, R., and Schnitzer, M.J. (2004). *In Vivo* Mammalian Brain Imaging Using One- and Two-Photon Fluorescence Microendoscopy. J. Neurophysiol. *92*, 3121–3133.

Kepecs, A., Uchida, N., Zariwala, H.A., and Mainen, Z.F. (2008). Neural correlates, computation and behavioural impact of decision confidence. Nature *455*, 227–231.

Kim, J.J., and Fanselow, M.S. (1992). Modality-specific retrograde amnesia of fear. Science *256*, 675–677.

Kim, C.K., Ye, L., Jennings, J.H., Pichamoorthy, N., Tang, D.D., Yoo, A.W., Ramakrishnan, C., and Deisseroth, K. (2017). Molecular and Circuit-Dynamical Identification of Top-Down Neural Mechanisms for Restraint of Reward Seeking. Cell *170*, 1013–1027.e14.

Kitamura, T., Ogawa, S.K., Roy, D.S., Okuyama, T., Morrissey, M.D., Smith, L.M., Redondo, R.L., and Tonegawa, S. (2017). Engrams and circuits crucial for systems consolidation of a memory. Science *356*, 73–78.

Lipton, P.A., Alvarez, P., and Eichenbaum, H. (1999). Crossmodal associative memory representations in rodent orbitofrontal cortex. Neuron *22*, 349–359.

Madisen, L., Garner, A.R., Shimaoka, D., Chuong, A.S., Klapoetke, N.C., Li, L., van der Bourg, A., Niino, Y., Egolf, L., Monetti, C., et al. (2015). Transgenic mice for intersectional targeting of neural sensors and effectors with high specificity and performance. Neuron *85*, 942–958.

McClelland, J.L., McNaughton, B.L., and O'Reilly, R.C. (1995). Why there are complementary learning systems in the hippocampus and neocortex: insights

from the successes and failures of connectionist models of learning and memory. Psychol. Rev. *102*, 419–457.

Miyamichi, K., Amat, F., Moussavi, F., Wang, C., Wickersham, I., Wall, N.R., Taniguchi, H., Tasic, B., Huang, Z.J., He, Z., et al. (2011). Cortical representations of olfactory input by trans-synaptic tracing. Nature *472*, 191–196.

Mombaerts, P., Wang, F., Dulac, C., Chao, S.K., Nemes, A., Mendelsohn, M., Edmondson, J., and Axel, R. (1996). Visualizing an olfactory sensory map. Cell *87*, 675–686.

Namboodiri, V.M.K., Otis, J.M., van Heeswijk, K., Voets, E.S., Alghorazi, R.A., Rodriguez-Romaguera, J., Mihalas, S., and Stuber, G.D. (2019). Single-cell activity tracking reveals that orbitofrontal neurons acquire and maintain a long-term memory to guide behavioral adaptation. Nat. Neurosci. *22*, 1110–1121.

Ostlund, S.B., and Balleine, B.W. (2005). Lesions of medial prefrontal cortex disrupt the acquisition but not the expression of goal-directed learning. J. Neurosci. *25*, 7763–7770.

Ostlund, S.B., and Balleine, B.W. (2007). Orbitofrontal cortex mediates outcome encoding in Pavlovian but not instrumental conditioning. J. Neurosci. *27*, 4819–4825.

Otis, J.M., Namboodiri, V.M.K., Matan, A.M., Voets, E.S., Mohorn, E.P., Kosyk, O., McHenry, J.A., Robinson, J.E., Resendez, S.L., Rossi, M.A., and Stuber, G.D. (2017). Prefrontal cortex output circuits guide reward seeking through divergent cue encoding. Nature *543*, 103–107.

Pachitariu, M., Steinmetz, N.A., Kadir, S.N., Carandini, M., and Harris, K.D. (2016). Fast and accurate spike sorting of high-channel count probes with KiloSort. In Advances in Neural Information Processing Systems 29, D.D. Lee, M. Sugiyama, U.V. Luxburg, I. Guyon, and R. Garnett, eds. (Curran Associates, Inc.), pp. 4448–4456.

Padoa-Schioppa, C., and Assad, J.A. (2006). Neurons in the orbitofrontal cortex encode economic value. Nature *441*, 223–226.

Pnevmatikakis, E.A., Soudry, D., Gao, Y., Machado, T.A., Merel, J., Pfau, D., Reardon, T., Mu, Y., Lacefield, C., Yang, W., et al. (2016). Simultaneous Denoising, Deconvolution, and Demixing of Calcium Imaging Data. Neuron *89*, 285–299.

Poo, C., and Isaacson, J.S. (2009). Odor representations in olfactory cortex: "sparse" coding, global inhibition, and oscillations. Neuron *62*, 850–861.

Price, J.L. (1985). Beyond the primary olfactory cortex: Olfactory-related areas in the neocortex, thalamus and hypothalamus. Chem. Senses *10*, 239–258.

Price, J.L., and Powell, T.P. (1970). The mitral and short axon cells of the olfactory bulb. J. Cell Sci. *7*, 631–651.

Ramus, S.J., and Eichenbaum, H. (2000). Neural correlates of olfactory recognition memory in the rat orbitofrontal cortex. J. Neurosci. *20*, 8199–8208.

Rennaker, R.L., Chen, C.F., Ruyle, A.M., Sloan, A.M., and Wilson, D.A. (2007). Spatial and temporal distribution of odorant-evoked activity in the piriform cortex. J. Neurosci. *27*, 1534–1542.

Ressler, K.J., Sullivan, S.L., and Buck, L.B. (1993). A zonal organization of odorant receptor gene expression in the olfactory epithelium. Cell *73*, 597–609.

Ressler, K.J., Sullivan, S.L., and Buck, L.B. (1994). Information coding in the olfactory system: evidence for a stereotyped and highly organized epitope map in the olfactory bulb. Cell *79*, 1245–1255.

Roesch, M.R., Stalnaker, T.A., and Schoenbaum, G. (2007). Associative encoding in anterior piriform cortex versus orbitofrontal cortex during odor discrimination and reversal learning. Cereb. Cortex *17*, 643–652.

Rossant, C., Kadir, S.N., Goodman, D.F.M., Schulman, J., Hunter, M.L.D., Saleem, A.B., Grosmark, A., Belluscio, M., Denfield, G.H., Ecker, A.S., et al. (2016). Spike sorting for large, dense electrode arrays. Nat. Neurosci. *19*, 634–641.

Roxin, A., and Fusi, S. (2013). Efficient Partitioning of Memory Systems and Its Importance for Memory Consolidation. PLoS Comput. Biol. *9*, e1003146.

Royer, S., Zemelman, B.V., Barbic, M., Losonczy, A., Buzsáki, G., and Magee, J.C. (2010). Multi-array silicon probes with integrated optical fibers: light-assisted perturbation and recording of local neural circuits in the behaving animal. Eur. J. Neurosci. *31*, 2279–2291.

Schoenbaum, G., and Eichenbaum, H. (1995). Information coding in the rodent prefrontal cortex. I. Single-neuron activity in orbitofrontal cortex compared with that in pyriform cortex. J. Neurophysiol. *74*, 733–750.

Schoenbaum, G., Chiba, A.A., and Gallagher, M. (1998). Orbitofrontal cortex and basolateral amygdala encode expected outcomes during learning. Nat. Neurosci. *1*, 155–159.

Schoenbaum, G., Chiba, A.A., and Gallagher, M. (1999). Neural encoding in orbitofrontal cortex and basolateral amygdala during olfactory discrimination learning. J. Neurosci. *19*, 1876–1884.

Schoenbaum, G., Nugent, S.L., Saddoris, M.P., and Setlow, B. (2002). Orbitofrontal lesions in rats impair reversal but not acquisition of go, no-go odor discriminations. Neuroreport *13*, 885–890.

Schultz, W. (2016). Dopamine reward prediction error coding. Dialogues Clin. Neurosci. *18*, 23–32.

Schwabe, K., Ebert, U., and Löscher, W. (2004). The central piriform cortex: anatomical connections and anticonvulsant effect of GABA elevation in the kindling model. Neuroscience *126*, 727–741.

Sosulski, D.L., Bloom, M.L., Cutforth, T., Axel, R., and Datta, S.R. (2011). Distinct representations of olfactory information in different cortical centres. Nature *472*, 213–216.

Squire, L.R., and Alvarez, P. (1995). Retrograde amnesia and memory consolidation: a neurobiological perspective. Curr. Opin. Neurobiol. *5*, 169–177.

Stalnaker, T.A., Franz, T.M., Singh, T., and Schoenbaum, G. (2007). Basolateral amygdala lesions abolish orbitofrontal-dependent reversal impairments. Neuron *54*, 51–58.

Stettler, D.D., and Axel, R. (2009). Representations of odor in the piriform cortex. Neuron *63*, 854–864.

Sugai, T., Miyazawa, T., Fukuda, M., Yoshimura, H., and Onoda, N. (2005). Odor-concentration coding in the guinea-pig piriform cortex. Neuroscience *130*, 769–781.

Takehara-Nishiuchi, K., and McNaughton, B.L. (2008). Spontaneous changes of neocortical code for associative memory during consolidation. Science *322*, 960–963.

Thorpe, S.J., Rolls, E.T., and Maddison, S. (1983). The orbitofrontal cortex: neuronal activity in the behaving monkey. Exp. Brain Res. *49*, 93–115.

Tremblay, L., and Schultz, W. (1999). Relative reward preference in primate orbitofrontal cortex. Nature *398*, 704–708.

Vassar, R., Chao, S.K., Sitcheran, R., Nuñez, J.M., Vosshall, L.B., and Axel, R. (1994). Topographic organization of sensory projections to the olfactory bulb. Cell *79*, 981–991.

Vong, L., Ye, C., Yang, Z., Choi, B., Chua, S., Jr., and Lowell, B.B. (2011). Leptin action on GABAergic neurons prevents obesity and reduces inhibitory tone to POMC neurons. Neuron *71*, 142–154.

Zhan, C., and Luo, M. (2010). Diverse patterns of odor representation by neurons in the anterior piriform cortex of awake mice. J. Neurosci. *30*, 16662–16672.

Zhang, X., and Firestein, S. (2002). The olfactory receptor gene superfamily of the mouse. Nat. Neurosci. *5*, 124–133.

STAR★METHODS

KEY RESOURCES TABLE

REAGENT OR RESOURCE	SOURCE	IDENTIFIER
Experimental Models: Organisms/Strains		
Mouse: wild type C57BL/6J	Jackson Laboratory	000664; RRID:IMSR_JAX:000664
Mouse: rosa26-loxp-stop-loxp-GCaMP6s	Jackson Laboratory	024106; RRID:SCR_002187
Mouse: Vglut2-ires-cre	Jackson Laboratory	016963; RRID:IMSR_JAX:016963
Software and Algorithms		
MATLAB	Mathworks	https://www.mathworks.com/; RRID:SCR_001622
MATLAB algorithm for registration within and across imaging sessions	Guizar-Sicairos et al., 2008	https://www.mathworks.com/matlabcentral/fileexchange/18401-efficient-subpixel-image-registration-by-cross-correlation
MATLAB algorithm for extracting cellular CA^{+2} signals	Pnevmatikakis et al., 2016	https://www.cell.com/neuron/fulltext/S0896-6273(15)01084-3
Custom MATLAB scripts for analyzing CA^{+2} signals	Mathworks	N/A
FIJI	University of Wisconson-Madison LOCI	http://fiji.sc/; RRID:SCR_002285
Python 3.6	Python	https://www.python.org/; RRID:SCR_008394
Scikit-Learn		https://scikit-learn.org/; RRID:SCR_002577
iPython and Jupyter		https://jupyter.org; RRID:SCR_018414
Other		
200 um, 0.39 NA optical fiber for optogenetics (mPFC)	Thorlabs	Custom Fabrication
200 um, 0.39 NA optical fiber for optogenetics (OFC)	Thorlabs	CFM12L02
0.5-mm GRIN lens	GRINTECH	NEM-050-50-00-920-S-1.5p
rAAV5-hSyn-eNPHR3.0-EYFP	University of North Carolina Vector Core	https://www.med.unc.edu/genetherapy/vectorcore/in-stock-aav-vectors/deisseroth/
rAAV5-hSyn-EYFP	University of North Carolina Vector Core	https://www.med.unc.edu/genetherapy/vectorcore/in-stock-aav-vectors/deisseroth/
rAAV5-hSyn-hChR2(H134R)-EYFP	University of North Carolina Vector Core	https://www.med.unc.edu/genetherapy/vectorcore/in-stock-aav-vectors/deisseroth/

RESOURCE AVAILABILITY

Lead Contact

Further information and requests for resources and reagents should be directed to and will be fulfilled by the Lead Contact, Richard Axel (ra27@columbia.edu).

Materials Availability

This study did not generate new, unique reagents.

Data and Code Availability

The datasets and code generated during this study are available upon request.

EXPERIMENTAL MODEL AND SUBJECT DETAILS

All experimental and surgical protocols were performed in accordance with the guide of Care and Use of Laboratory Animals (NIH) and were approved by the Institutional Animal Care and Use Committee at Columbia University. For all head-fixed behavior and

inhibition experiments, Vglut2-ires-cre mice (Vong et al., 2011) were crossed to Ai96 (Madisen et al., 2015), and all male and female heterozygous transgenic offspring aged 8-16 weeks were used. For all freely-moving behavior and inhibition experiments, C57BL/6J male mice aged 8-16 weeks were used. All animals were maintained under a normal 12 hour light/dark cycle with littermates until implantation of optical fibers or GRIN lenses.

METHOD DETAILS

Stereotaxic Surgeries

Mice were anesthetized with ketamine (100 mg/kg) and xylazine (10mg/kg) through intraperitoneal injection and then placed in a stereotactic frame. Body temperature was stabilized using a heating pad attached to a temperature controller. For lens implantation experiments, a 1.0-1.5mm round craniotomy centered on the implantation coordinate was made using a dental drill. The following coordinates were used (mm): piriform cortex, ML: 1.2; AP: 2.2; DV: −3.35; OFC, ML: 1.0; AP: 2.3-2.4; DV: −2.45; mPFC, ML: 0.4; AP: 1.65; DV: −2.05. Dura and 0.5mm – 1mm of underlying cortex was then aspirated. We note that mice with motor cortex aspirations and GRIN lens implantations were not deficient in learning compared to YFP animals in which a fiber optic was implanted without cortical aspiration (Figure 1C versus Figures 4B and 4C). A 0.5mm diameter and 6.4 mm length microendoscope was then inserted. After implantation, the microendoscopes were fixed in place using Metabond (Parkell) onto the exposed region. To protect the lens a metal enclosure was placed around it (Dytran thread adaptor) and covered with an acorn nut (Amazon). Lastly, a custom-made head plate (stainless steel) was attached to the skull with Metabond to allow for head-fixation.

For optical fiber implantation experiments, virus was first injected using a micropipette that was made using a Sutter Micropipette Puller (P-2000). All viruses were purchased from UNC Vector Core. Volumes were injected at 100 nL per minute (see Table S4 for virus and injection information). The following coordinates were used (mm): piriform cortex, ML: 2.75; AP: 1.3; DV: −4.75; OFC, ML: 1.0; AP: 2.3-2.4; DV: −2.45; mPFC, ML: 0.4; AP: 1.65; DV: −2.05. Afterward, 0.39-NA optical fibers (Thorlabs) were implanted bilaterally 0.35mm above the DV virus injection coordinate. Following surgery, mice received buprenorphine (0.05 - 0.1 mg/kg) subcutaneously every 12 hours over the next three days. Mice recovered for at least 4 weeks before the start of any imaging or optogenetic experiment.

Animal Behavior

Mice were water-restricted (water bottles taken out of cage) and received water (bottle placed back into cage) for 4-5 minutes every day. Behavioral training began when mice weighed less than 90% of free drinking weight (~3 days for all experiments). Mice were also weighed every day to ensure good health. No health problems related to dehydration arose at any point.

Head-fixed behavior

Mice did not undergo any form of shaping prior to assessment of a learning deficit during either the single-phase learning task (Figure 4) or the pre-training phase of the two-phase learning task (Figure 5). Mice were head-fixed on a large 20 cm diameter Styrofoam ball, where they could run freely forward and backward (Video S1). To assess locomotion, the axis of the treadmill was attached to an analog rotary encoder (US Digital part #: MA3-A10-125-B), and angular velocity was measured. During imaging, mouse behavior was monitored with an IR camera (Point Grey). A custom olfactometer was made with mass flow controllers (Aarlborg) and quiet solenoid valves (Lee Company), which were controlled by a USB-DAQ (Measurement Computing) using high voltage transistor arrays. The odor stream was set to 800 mL/min, and split into two equal lines carrying 400 mL/min (see Table S2 for list of odorants used). One line delivered odors through a narrow opening placed next to the animal's nose to allow for odor sampling. The other line was connected to a photo-ionization device (Aurora Scientific) to measure odor ionization, an indicator of odor identity and concentration. Water was delivered through a quiet solenoid-controlled valve (Lee Instruments) to a lick port (gavage needle) irrespective of whether the animals engaged in anticipatory licking. Licking events were collected through a capacitive touch sensor (Phidgets) attached to the lick port. Behavioral training and data acquisition were accomplished with custom MATLAB scripts. All data was collected at 1000 Hz.

Most mice learned instantly, without any prior training, to lick from a lick port to collect water. Each odor trial had the following structure: 5 s baseline, 2 s odor, 3 s delay, followed by water in CS+ trials. The inter-trial interval was 25 s. During pre-training, one CS+ odor was presented. Animals collected water in greater than 95% of CS+ trials (Figure 4D). However, in the rare cases when water was not collected, the next trial was halted until water was collected during the inter-trial interval. In most experiments, octanol served as the CS+ odor during pre-training, and methyl salicylate and pinene served as the CS+ odors, and eucalyptol and limonene served as CS- during discrimination learning. Each day of pre-training consisted of 40-60 trials of the single CS+ odor. Discrimination training consisted of five types of trials, delivered pseudo-randomly: 2 CS+ odors that predicted water delivery, 2 CS- odors, and US trials in which water was delivered without prior odor delivery. Each day of discrimination training consisted of 12-15 trials of each of the 5 conditions (60-75 trials total). Passive odor exposure consisted of odors being delivered without the presence of a lick port. For imaging experiments, most training sessions were conducted every other day to minimize GCaMP6s bleaching.

For bilateral photo-inhibition experiments, a 560 nm laser (CrystaLaser) was used for mice expressing either the halorhodopsin NpHR or YFP. The laser was connected through a single patch cord and a rotary joint (Doric Lenses) to divide the laser output equally onto bilaterally implanted optical fibers. The power at the end of each fiber tip was approximately 8-10 mW for all inhibition

experiments. The laser was turned on 2 s prior to odor delivery and turned off 2 s after US delivery, lasting for a total of 9 s. The laser was also on for 9 s in CS- trials. For unilateral photo-excitation experiments, a 473 nm laser (CrystaLaser) was used for mice expressing ChR2. The power at the end of the fiber tip was 2-4 mW. Laser photoillumination was delivered for 2 s, the same amount of time as odor delivery. To confirm that the optical fibers had delivered the expected amount of power during the experiment, implanted fibers were extracted immediately after perfusion and output power levels at the fiber tip were re-tested.

Freely-moving behavior

Mice did not undergo any form of shaping prior to photoillumination during the pre-training phase of the two-phase task. Water-restricted animals were placed in a 1ft x 1ft training chamber and allowed to explore freely. The training chamber was placed in a sound-attenuating PVC cabinet (MedAssociates) and was retrofitted with a custom-made ceiling with a holder (Thorlabs) for a 1 to 2 intensity splitter rotary joint (Doric Lenses) that allowed free movement of the animal during laser photoillumination sessions. The training chamber had a custom-made nose port on one wall. The nose port contained a lick spout (gavage needle) connected to a capacitive touch sensor (Phidgets), a vacuum line connected to wall vacuum, and an odor line connected to the olfactometer. The behavioral training was monitored with an IR camera (Point Grey). All behavioral training was controlled with custom-written Python scripts. Entry of the animal nose into the nose port was detected with IR sensors (Sparkfun).

A behavioral training session lasted approximately 30 minutes and an animal could complete as many as 200 trials. For optogenetic silencing experiments, the laser was turned on for the entire training session. The laser output was divided equally to the bilaterally implanted optical fibers. The laser power was adjusted such that the power measured at each fiber tip was between 10-15 mW for all inhibition experiments. Odors (diluted to 1% with mineral oil) were pinene (pre-training CS+), isoamyl acetate (discrimination CS+), and ethyl acetate (discrimination CS-). Odors were delivered with a custom made olfactometer (with parts from Lee Instruments) and an air pump (MedAssociates) at a rate of 1 L/min. Trials of CS+ and CS- odors were delivered in a pseudo-random order. The trial structure was as follows: the trial was initiated when the animal inserted their nose into the nose port, as detected by the IR sensor. After 0.7 s, if the animal was still in the port (as reported by the IR sensor), the odor was delivered for 2.4 s, followed immediately by water if the odor was a CS+ odor. Each trial was followed by a 5 s inter-trial interval during which no trials could be initiated. Behavioral performance was quantified by measuring the percent of time of contact between the animal and the sipper in the 1.2 s interval before the end of odor delivery.

We note that non-lick contacts, manifested as continuous touch events, were extensive. Therefore, the lick port is measuring contact, and we defined anticipatory behavior as the total time of contact between the animal and the lick port. This behavior does not occur in CS- trials after learning (Figures S6H–S6J).

Head-fixed Imaging

A two-photon microscope (Ultima, Bruker) was equipped with the following components to allow imaging of deep brain areas *in vivo*: a tunable mode-locked 2-photon laser (Chameleon Vision, Coherent) set to 920 nm, ~100 fs pulse width; a GaAsp-PMT photo-detector with adjustable voltage, gain, and offset feature (Hammatsu Photonics); a single green/red NDD filter cube (580 dcxd dichroic, hq525/70 m-2p bandpass filter); a long working distance 10X air objective with 0.3 NA (Olympus).

A 260 pixel X 260 pixel region of interest (~400 um X 400 um FOV) was chosen, with 1.6 us dwell time per pixel, to allow image collection at 4.5 Hz. Imaging of the same plane (z axis) was accomplished across multiple days by using the top of the GRIN lens as a reference point. Images were then acquired at depth increments of 5-10 um and the mean intensity image for each depth was aligned to a reference image. For each trial, two-photon scanning was triggered at the onset of the baseline period (5 s prior to odor delivery), and a 19 s (75 frames) video was collected. Data was acquired using custom acquisition software (Bruker Instruments).

Optrode Experiments

Extracellular recordings were performed acutely in head-fixed animals using 32-channel silicon probes (Buzsaki32, NeuroNexus) with a 100 um core fiber attached to one of the four shanks. A 560nm laser was used for halorhodopsin activation. Recordings were performed 4 weeks after virus injection. On recording days, mice were anesthetized with ketamine/xylazine, the skull indentation created during virus injection was enlarged using a drill, and the dura was removed. Subsequently, mice were head-fixed to the recording stage, and the optrode was lowered inside the brain with a micro-manipulator. The incision was then sealed with liquid agar (1.5%) applied at body temperature.

We lowered optical fibers down to 2-3 mm below Bregma toward the OFC and performed a series of recordings during photoillumination with several laser power levels (.5 mW, 1 mW, 2 mW, 5 mW, 10 mW, and 15 mW, measured at fiber end). For each power level, the laser was turned on for 10 s with an ITI of 30 s for a total of 15 consecutive trials. In halorhodopsin-expressing animals, we also performed longer trials of photo-illumination (10min) to mimic the freely moving silencing protocol.

The 32-channel recording data were digitized at 40 KHz and acquired with OmniPlex D system (Plexon Inc). The voltage signals were high-pass filtered (200 Hz, Bessel) and sorted automatically with KlustaKwik (Rossant et al., 2016) or Kilosort (Pachitariu et al., 2016). The clusters were then manually curated with KlustaViewa or Phy GUI to merge spikes from the same units and to remove noise and units that were not well isolated. Spike data were converted into firing rates using a first-order Savitsky-Golay filter with a smoothing window of 100 ms.

Histology

Mice were euthanized after anesthesia with ketamine/xylazine. Brains were extracted and incubated in PFA for 24 hours, and coronal sections (100 um) were cut on a vibratome (Leica). The sections were incubated with far-red neurotrace (640/660, Thermo Fisher Scientific) to label neuronal cell bodies. All images were taken using a Zeiss LSM-710 confocal microscope system. Histology was performed to confirm locations of implanted lenses and optical fibers, as well as expression levels for GCaMP6, YFP, channelrhodopsin and halorhodopsin.

RNA-scope

Mice were euthanized after anesthesia with ketamine/xylazine. Brains were extracted, submerged in O.C.T., immediately frozen in −80C 2-methylbutane and stored in airtight containers until sectioning. Coronal sections (16um) were cut on a cryostat, collected on Thermofisher Superfrost slides and stored in an airtight container at −80C. Sections were processed with the RNAscope Fluorescent Multiplex Assay, with standard methods. Sections were labeled with probes for vGlut1, vGlut2 and GCaMP, counterstained with DAPI, and imaged with a Zeiss LSM-710 confocal microscope system using 20x magnification. An average of 300 cells per brain region (piriform, OFC and mPFC) were assayed for the presence of vGlut1, vGlut2 and GCaMP signals across multiple coronal sections.

Data Collection and Exclusion

Investigators were not blind during either imaging or optogenetic experiments. For imaging experiments, mice were excluded if the field of view contained less than 20 neurons, if the signal was too dim, or if the lens was not placed directly above the region of interest (n = 1, Cohort C). For optogenetic experiments, mice were excluded based on the following criteria: if histology revealed low opsin expression within the region of interest (n = 4, all conditions), if histology revealed brain damage (n = 3, all conditions), if the optic fibers were not located at the target coordinate (n = 10, all conditions), or if the optic fibers did not transmit excitation light properly (n = 0, all conditions). 1 mouse was excluded from both cohorts U and V due to failure to learn pretraining in the two-phase task (see Table S3).

QUANTIFICATION AND STATISTICAL ANALYSIS

Image processing and calcium transient analysis were performed using MATLAB. Significance was defined as $p < 0.05$. All statistical tests, behavioral data analyses and imaging data analyses were performed using Python. Wilcoxon rank-sum test (two-tailed) was used in two-group comparisons, and Wilcoxon signed-rank test (two-tailed) was used in paired group comparisons. For multiple-group comparisons, a Kruskal-Wallis test was first performed on group data, and, following rejection of the Kruskal-Wallis test, a post hoc Dunn's test of Multiple Comparisons was performed to evaluate significance between pairs of groups.

Behavioral Data Analysis

For head-fixed behavior, anticipatory licking was defined to be the number of licks within the 1.0 s window prior to water delivery, and collection licking was defined as the number of licks in the 1.0 s after water delivery. For freely-moving behavior, anticipatory contact behavior was defined as the percentage of time of contact between the animal and the sipper in the last 1.2 s prior to water delivery, and collection contact behavior was defined as the percentage of time of contact between the animal and the sipper in the 1.2 s after water delivery. AUC (area under ROC) was calculated for each mouse by comparing the distributions of licks in CS+ trials and in CS- trials using a rolling average with a length of 20 trials.

To quantify trials to criterion, we calculated the percent of trials with anticipatory licks using a moving average. Trials to criterion for licking to CS+ odors was defined as the number of trials to reach anticipatory licking in over 80% of CS+ odor trials. Trials to criterion for the suppression of licking to CS- odors was defined as the number of trials to display anticipatory licking in less than 20% of CS- odor trials. The length of the moving average filter was adjusted to match the differences in duration to learn in the different tasks. Length of moving average for single-phase head-fixed task = 20; the pre-training phase of the two-phase head-fixed task = 20; the discrimination phase of the two-phase head-fixed task = 10; the pre-training phase of the two-phase freely moving task = 40; and the discrimination phase of the two-phase discrimination task = 20.

Image Processing

Images were first motion corrected using sub-pixel image registration (Guizar-Sicairos et al., 2008). Motion correction was first applied within each trial (75 frames per trial), and then across trials by registering the mean intensity image of different trials (40-80 trials per imaging session). In some FOVs, we often observed small fluorescence changes occurring in large areas (> 100 um X 100 um) that could be the consequence of calcium transients in out-of-focus planes. We eliminated these diffuse calcium fluctuations through a spatial low-pass Gaussian filter prior to calcium transient analysis (length constant, 50 um) (Video S2).

Calcium Transient Analysis

For ROI identification, we used a MATLAB package for calcium transient analysis based on nonnegative matrix factorization (NMF) (Pnevmatikakis et al., 2016). ROIs that corresponded to neurons were selected, and other signals (i.e., from neuropil) that did not correspond to neural cell bodies were deleted. On rare occasions, the algorithm classified distinct neurons in close proximity as

one neuron, and we split the spatial filters manually. On average, 70-100 neurons were extracted, and de-noised DF / F was computed using the NMF algorithm.

To identify the same neurons across multiple days of imaging sessions (Video S3), we first used a MATLAB rigid body registration and sub-pixel registration algorithm on the mean intensity averages of image stacks collected on different days. We then applied the angular rotation and translation to both the image stacks and the ROIs on different days to register image stacks across days. For example, for a set of imaging data acquired across 5 days, we used day 3 as reference, and all image stacks on other days were registered relative to day 3. Subsequently, we manually pooled all unique and spatially non-overlapping cells identified across all imaging days to produce a large set of ROIs, or spatial filters. Neuronal cell counts obtained after this step typically exceeded standard single-day cell count results by 20%–40%.

We then back-applied these spatial filters to each imaging day to derive the best spatial filter for all imaging days. Sometimes, the back-application process resulted in spatial filters that did not correspond to the same cell on different imaging days. We thus visually assessed whether the back-applied spatial filters corresponded to the same cell on different days. We evaluated the shapes of the spatial filters while being blind to the fluorescence data and spatial location of the cell, and chose only cells for which spatial filters on multiple days appeared to correspond to the same outline. This usually led to the exclusion of 20% of all ROIs from the master list when aligning across 4 or more imaging days.

Quantification of Significant Neuronal Responses

Odor responses were analyzed during the 5 s between odor onset and water onset, spanning 2 s of odor delivery and 3 s of delay before water onset. This time window was chosen to encompass all odor-evoked activity after odor onset, including responses present throughout the delay period. We ended the analysis window at water onset to exclude water responses.

For each cell, we pooled all the DF/F values of all trials during the baseline period (the first five seconds of each imaging trial) to create a reference distribution. This was compared to a test distribution of pooled DF/F values with a moving window of 3 frames (0.67 s). A Mann-Whitney U test was performed on the reference and test distributions to obtain a P value. With this method, a P value was obtained for every frame after odor onset. A cell was defined as significantly active on a given imaging day only 1) if the P value was < 0.01 for at least 8 consecutive frames within the 5 s period ($\sim$22 frames) between odor onset and water delivery, and 2) if the maximum DF/F during the odor delivery period exceeded the DF/F during the baseline period over a set threshold. This DF/F threshold was 0.10 for piriform responses, 0.04 for OFC responses, and 0.03 for mPFC responses to account for varying degrees of GCaMP6S expression within each area. We used this metric to quantify the fraction of cells responsive to a stimulus on a given imaging day as well as to compare the activities of cells within and across days. The onset of a significant odor response was calculated by finding the first frame with a P value less than 0.01.

It was often the case that responses to the old CS+ odors did not diminish completely to baseline in OFC neurons after reversal learning. We thus quantified the fraction of neurons that responded more to CS+ than to CS- odors and vice versa, after discrimination learning and after reversal learning. Neurons were considered to be responding more to CS+ than CS- odors, if they had statistically significant responses to both CS+ odors and also had higher amplitude responses to CS+ odors than to CS- odors.

Response Power

We defined the excitatory response power to a given odor as the mean amplitude of the excitatory population response to that odor. Likewise, we defined the inhibitory response power to a given odor as the mean amplitude of the inhibitory population response to that odor. A neuron's trial-averaged odor response was included in the excitatory population on a given imaging day (for example, Figure 2E), or in a given window of trials (for example, as in Figure 2D), if the mean response in the interval between odor onset and water onset was greater than 0.0 DF/F. Likewise, it was included in the inhibitory population if its mean response was less than 0.0 DF/F. A given neuron could thus be included in the calculation for excitatory power on a given day and for inhibitory power on different day, depending on its activity. To quantify response power as a function of trials across multiple imaging days, response power was computed using a moving window of 13 trials and was subsequently smoothed using a Savitzky-Golay filter with a length of 3 trials.

Correlation Analysis

To calculate the correlation within an odor (diagonal entries of Figure 1I, for example), trials for a given odor were first randomly split into two equal halves. The maximum trial-averaged DF/F response between odor onset and water onset for all neurons was computed by creating two vectors that corresponded to the average odor-evoked population activity of the two splits. The Pearson product-moment correlation coefficient was then calculated using the two population activity vectors. This was repeated 100 times and the average correlation was computed. To calculate the correlation between two different odors (off-diagonal entries of Figure 1I, for example), all trials for each odor were once again assigned randomly to one of two equal sets. One set was selected for each odor, and the correlation was calculated using the two population activity vectors, as before. To calculate the correlation of excitatory responses (Figure 1K, for example), all inhibitory values in the population activity vector were replaced with zeros. To calculate the correlation of inhibitory responses (Figure 1K, for example), all excitatory values in the population activity vector were replaced with zeros.

Decoding

Support vector machines with linear kernels were constructed using the scikit-learn library in Python. For each odor trial we created a vector that corresponds to the population activity based on the maximum DF/F between odor onset and water onset for each trial. The number of neurons used was standardized across all animals and all conditions as n = 40 neurons. Neurons were chosen randomly. For decoding of odors across days, we trained the decoder using all trials from a given day and tested the decoder with trials on each of the other days. For decoding of odors within the same day, we trained the decoder using 5-fold cross-validation. Decoding simulations were repeated 100 times per condition by drawing a new and random set of 40 neurons.

For decoding odor value, CS+1 and CS+2 odor trials were pooled together, CS-1 and CS-2 odor trials were pooled together, and each pool had a different label. For decoding CS+ odor identity, CS+1 trials and CS+2 trials were used and had different labels. For decoding CS- odor identity, CS-1 trials and CS-2 trials were used and had different labels. For decoding odor identity, CS+1, CS+2, CS-1, and CS-2 trials were used and had different labels. The default strategy used for multi-class decoding of odor identities is the ''one-against-one'' multi-class classification approach. Chance performance for each of these conditions using random shuffling with 50 repetitions were: odor value 50%, CS+ identity 50%, CS- identity 50%, odor identity 25%.

The decoding of CS+ error trials was performed on training sessions after learning performance had plateaued. For each day after learning, a decoder was trained to discriminate between CS+ trials in which the animal displayed anticipatory licking and CS- trials in which the animal displayed no anticipatory licking. The 5-fold cross-validated training accuracy was used as a control. After the decoder was trained, it was tested on CS+ error trials in which there was no anticipatory licking. Decoding simulations were repeated 100 times per condition, drawing a new and random set of 40 neurons for each condition. This decoding analysis was also performed using only neurons that were activated during water collection in US-only trials. In this case, 10-15 neurons were generally responsive to US for a given mouse, and all neurons were used to train the decoder. Decoding was not performed if there were less than 7 neurons responsive to US in an imaging session.